Volume 19
DOE/DP40124-43

LLE Review

Quarterly Report

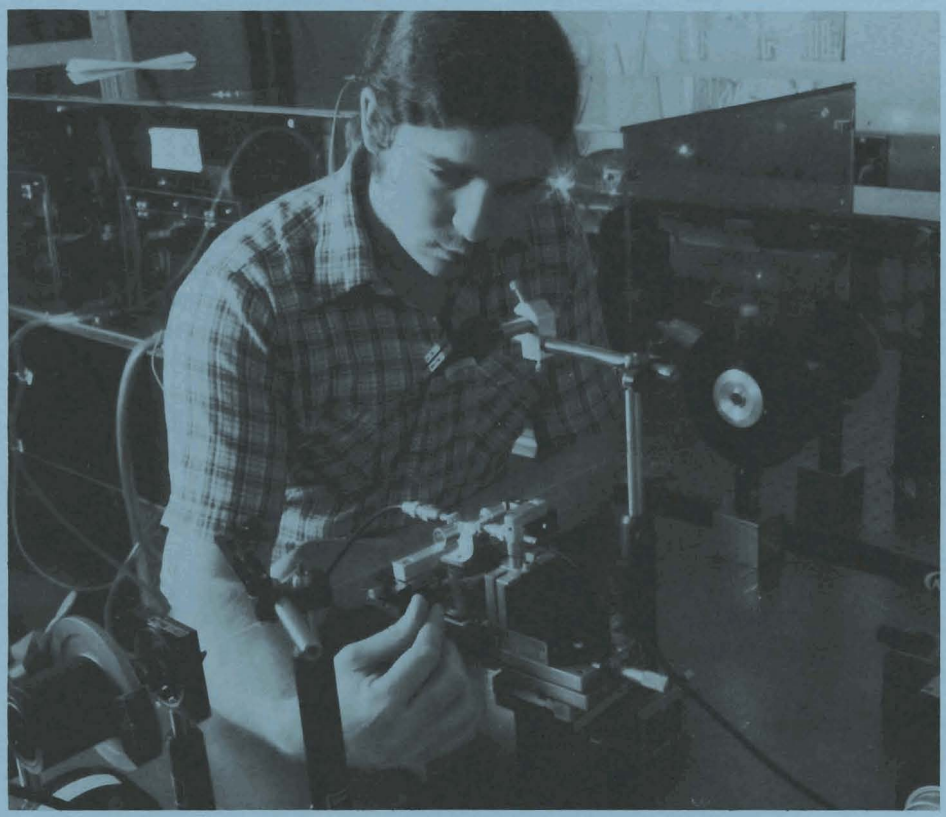

April–June 1984

Laboratory for Laser Energetics
College of Engineering and Applied Science
University of Rochester
250 East River Road
Rochester, New York 14623

Volume 19
DOE/DP40124-43

LLE Review

Quarterly Report

Editor: L. Iwan
(716) 275-5314

April–June 1984

Laboratory for Laser Energetics
College of Engineering and Applied Science
University of Rochester
250 East River Road
Rochester, New York 14623

This report was prepared as an account of work conducted by the Laboratory for Laser Energetics and sponsored by Empire State Electric Energy Research Corporation, General Electric Company, New York State Energy Research and Development Authority, Northeast Utilities Service Company, Southern California Edison Company, The Standard Oil Company, University of Rochester, the U.S. Department of Energy, and other United States government agencies.

IN BRIEF

This volume of the LLE Review contains articles on the activities in the GDL and OMEGA laser facilities, new theoretical and experimental developments in the physics of laser-produced plasmas, uniformity calculations for a direct-drive fusion reactor, technological advances in picosecond-measurement techniques, and NLUF activities during this quarter (April–June 1984).

Some highlights of these articles are

- A new model has been proposed for the Raman spectra observed in laser experiments. This model predicts an appreciable "up-scattered" spectral component which has now been observed.

- Recent UV-laser/plasma interaction experiments have significantly extended our understanding of the coronal plasma. In particular, some prominent features of the coronal spectra are shown to be especially suitable for diagnosing the coronal electron temperature.

- An analytical study of illumination uniformity has been carried out for direct-drive fusion reactors, using up to 96 laser beams to irradiate the fuel pellet. By increasing the number of beams, the illumination uniformity is made less sensitive to beam perturbations.

- Coplanar strip lines have replaced balanced transmission lines in the LLE sampling system to measure fast electrical transients. Fabrication is simpler and temporal resolution is already equal to the best attained previously.
- A high-repetition-rate pulsed laser source with extremely stable output energy has been built and characterized. This source substantially improves our capability to measure rapid transient phenomena.

In addition, the University of Rochester's Trustees' Visiting Committee for Major Projects and Programs reviewed the laboratory in February. The committee reports to the president of the university on all major university programs. Members of the committee who participated in the LLE review were Messrs. G. Poke, D. Potter, C. W. Rea, L. Simon, and C. Chandler (chairman). The laboratory received a highly favorable report from the committee — "... We congratulate the LLE leadership and university administration on the achievements of the last two years..."

CONTENTS

		Page
IN BRIEF		iii
CONTENTS		v
Section 1	LASER SYSTEM REPORT	101
1.A	GDL Facility Report	101
1.B	OMEGA Facility Report	102
Section 2	PROGRESS IN LASER FUSION	104
2.A	A New Model of Raman Spectra in Laser-Produced Plasma	104
2.B	Diagnostic Value of Odd-Integer Half-Harmonic Spectra	110
2.C	Illumination Uniformity Considerations for Direct-Drive Fusion Reactors	120
Section 3	ADVANCED TECHNOLOGY DEVELOPMENTS	129
3.A	Subpicosecond Electro-Optic Sampling Using Coplanar Strip Transmission Lines	129
3.B	An Ultra-Stable Nd:YAG-Based Laser Source	133
Section 4	NATIONAL LASER USERS FACILITY NEWS	139
PUBLICATIONS AND CONFERENCE PRESENTATIONS		

Optical alignment of the subpicosecond electro-optic sampling system is fine tuned by Kevin Meyer, a graduate student in physics and a member of the Picosecond Research Group. The system is used to study ultrafast electrical signals.

Section 1
LASER SYSTEM REPORT

1.A GDL Facility Report

The glass development laser (GDL) continued in its role as a UV interaction facility, supporting various programs such as damage testing of optical coatings, several interaction experiments for graduate students, x-ray biophysics and photolithography experiments, holographic beam characterization experiments, and active mirror characterization experiments. Operations personnel from GDL participated in engineering activities on the 25th-beam project — in particular, the Kuizenga oscillator development and active mirrors. Also, operations personnel became involved for the first time in the short-pulse UV probe project.

A summary of GDL operations this quarter follows:

Interaction Shots	87
X-Ray Target Shots	42
Damage-Testing Shots	303
Pointing, Calorimetry Shots	103
TOTAL	535

ACKNOWLEDGMENT

This work was supported by the U.S. Department of Energy Office of Inertial Fusion under contract number DE-AC08-80DP40124 and by the Laser Fusion Feasibility Project at the Laboratory for Laser Energetics which has the following sponsors: Empire State Electric Energy Research Corporation, General Electric Company, New York State Energy Research and Development Authority, Northeast Utilities Service Company, Southern California Edison Company, The Standard Oil Company, and University of Rochester. Such support does not imply endorsement of the content by any of the above parties.

1.B OMEGA Facility Report

OMEGA operations for this quarter consisted of work in four areas:

- support for several planned experimental campaigns,
- continued manufacturing engineering for the approaching up-conversion of six more OMEGA beamlines,
- procurement activities for the conversion of six additional beams to the UV, scheduled for late fall, and
- engineering support for the 25th-beam project.

Among the experimental campaigns carried out during this quarter were a continuing effort on the uniformity campaign in which equivalent-target-plane photographs were taken to observe the effects of deliberately imposed amplitude modulation of the beams; the thermal-transport studies program; coronal physics; implosion studies, including implosions on very high-aspect-ratio targets; diagnostic development; and two successful NLUF campaigns for users from the U.S. Naval Research Laboratory and the University of Hawaii.

Approximately half of the operations group has been participating in engineering efforts to provide the necessary assemblies to up-convert the second set of six OMEGA beams to the UV. As the quarter neared completion, most of the mechanical assemblies had been prepared for insertion into the laser system when the experimental campaigns are completed in July 1984. Optics for the next six beams are due in July or August, with cell assembly completion scheduled for September. Activation of the next six beams is planned for September, with 12-beam implosions slated to begin in October.

The procurement activities for the next set of six beams have begun during this quarter. Near the end of the quarter the components for the next set will be ordered.

Engineering activities of the group have been centered on the 25th-beam project. The development of Kuizenga oscillators for both OMEGA and GDL continued this quarter with activation of the pre-driver amplifier, activation of the second, active mode-locked, Q-switched oscillator, and redesign of the electronic control packages. The design has been completed for the upgraded OMEGA driver line with activation slated to occur in November. Other areas of engineering activity by the operations group include support of the active-mirror project with the first test-firings occurring this quarter; installation of the active mirrors in GDL is scheduled for the next quarter. A major software engineering project was completed this quarter involving simultaneous acquisition and reduction of data from four streak cameras with optical multi-channel analyzers.

Laser performance has improved as a result of concentrated efforts to improve beam balance and continued efforts to improve measurement accuracy of the calorimetry system. Furthermore,

replacement of the original turning mirrors has improved transport of the UV beams to the target. We were able to consistently place well over 300 J on target, with a high of 388.8 J (for 441 J out of the laser). Beam balance has been particularly impressive, well under the 5% that has been routinely achieved. Our best beam balance this quarter was 2.2% (with 364 J on target), and the average beam balance has been in the vicinity of 4%.

A summary of system activities this quarter follows:

Target Shots	272
System Test	102
Driver Test and Alignment	90
Beamline Testing, etc.	31
TOTAL	495

ACKNOWLEDGMENT

This work was supported by the U.S. Department of Energy Office of Inertial Fusion under contract number DE-AC08-80DP40124 and by the Laser Fusion Feasibility Project at the Laboratory for Laser Energetics which has the following sponsors: Empire State Electric Energy Research Corporation, General Electric Company, New York State Energy Research and Development Authority, Northeast Utilities Service Company, Southern California Edison Company, The Standard Oil Company, and University of Rochester. Such support does not imply endorsement of the content by any of the above parties.

Section 2
PROGRESS IN LASER FUSION

2.A A New Model of Raman Spectra in Laser-Produced Plasma

Recent experiments have studied the spectral and temporal distribution of scattered light from planar and spherical laser-produced plasmas.[1-4] The reradiation at $\omega_0/2$ (where ω_0 is the incident frequency) shows two relatively sharp increases when plotted as a function of increasing incident intensity.[2] These rises can be interpreted as the onset of the two-plasmon instability ($2\omega_p$) and then the absolute stimulated Raman scattering (SRS-A), respectively, occurring near the quarter-critical ($n_c/4$) surface in the plasma. Observation of a separated, broad band of radiation, lying in frequency between ω_0 and $\omega_0/2$, has been interpreted as evidence of the onset of the convective stimulated Raman instability (SRS-C) originating in the underdense region below $n_c/4$. The upper limit of this band corresponds to scattering from regions whose densities are as low as 0.05 n_c and the lower part to regions with densities as large as 0.2 n_c. Experimental observations of these two radiation features are shown in Figs. 19.1 and 19.2.[2,4]

There have remained some difficulties in this SRS-C interpretation. One is the observation that the broadband radiation sets in at almost the same intensity as the SRS-A, despite the theoretical prediction that the convective threshold should be considerably higher if both instabilities occur in plasma with comparable density scale lengths. A second is the existence of the two gaps in the spectrum, one between the lower end of the band and $\omega_0/2$, and the other between the upper end and ω_0. While the upper gap can be understood on

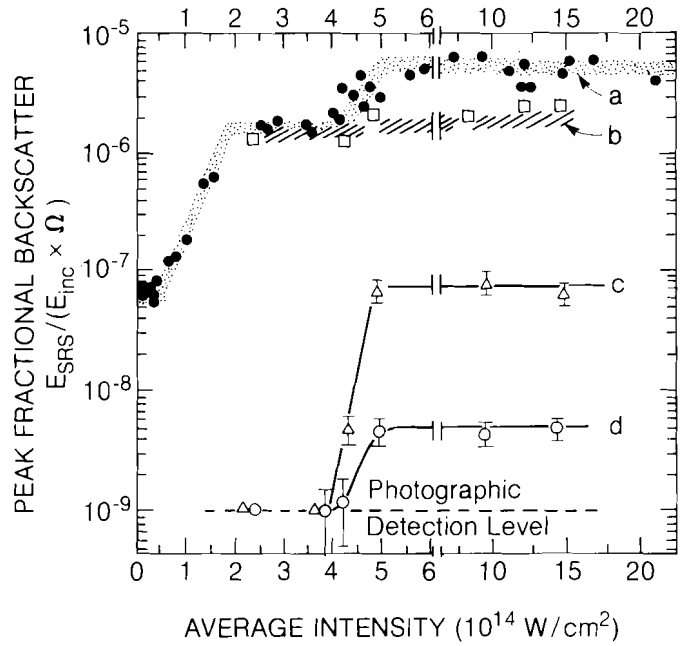

Fig. 19.1
Variation of the experimentally observed scattering with incident intensity. Curves "a" and "b" are the measured $\omega_o/2$ components with polarization parallel and perpendicular, respectively, to the incident laser polarization. Curve "c" represents backscattering at 500 nm (between $\omega_o/2$ and ω_o); curve "d" represents backscattering at $\omega_o/2$. The vertical axis for these last two curves is not absolutely calibrated.

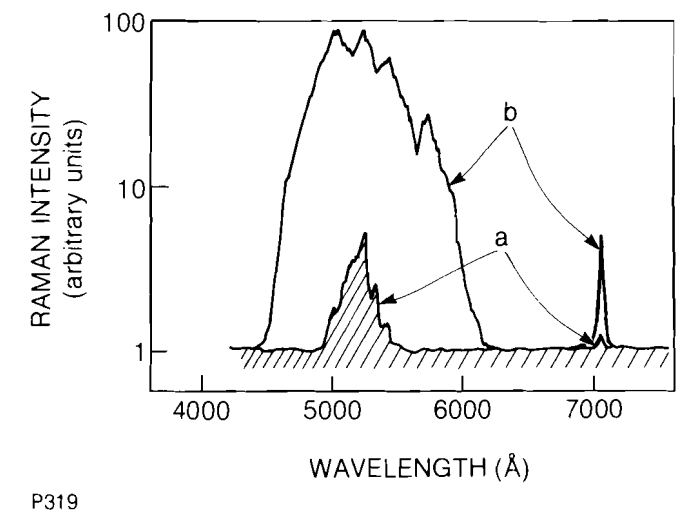

Fig. 19.2
Experimentally observed irradiation at $\omega_o/2$ and in the ω_o-$\omega_o/2$ band. Incident irradiation (ω_o) with 3510-Å laser-light threshold response is labeled "a." At higher incident intensities the response increases as in "b."

the basis of Landau damping,[4] the lower gap requires invocation of density steepening near $n_c/4$.[2] This is despite the fact that the lower gap is always present in a variety of experimental situations, some of which show little evidence of steepening.

A third difficulty is that some limited observations[5] of the azimuthal angular distribution show little variation, while SRS-C calculations, using spatial gain from noise sources, incorporate angular terms in the exponential factors[4] and lead to the prediction of strong peaking out of the plane of polarization. Finally, a fourth problem is that spectrally and temporally resolved data[2,4] show that the scattering in the band region does not generally occur over large regions of frequency and/or time simultaneously. The effect is one of scintillation, suggesting contributions from localized regions during brief periods of time.

One approach to explain these difficulties has been to invoke the creation of filaments by self-focusing of hot spots of the incident light.[3,4] The greatly increased light intensity in the filament can exceed the threshold for SRS-C. The scintillation in time may be due to instability of the filaments themselves, while the spatial localization may be due to the existence of a density peak along the filament length.

In this note we propose an alternative explanation of the spectral band based on ordinary incoherent Thomson scattering. It is well known that incoherent scattering of radiation from plasma[6] exhibits a number of interesting features, including a Doppler-broadening characteristic of the ion temperature near the incident frequency ω_o, and a sharp intense "plasma line" near the frequencies $\omega_o \pm \omega_p$ (Raman scattering). While the total scattered power in the plasma line is usually small compared with the incident power for a Maxwellian distribution of electrons, it can be much enhanced — as noted by Perkins and Salpeter.[7] In certain regions of the ionosphere, a two-temperature electron distribution is created in the daytime by absorption of the solar ultraviolet and x-rays, producing energetic photoelectrons in the 1- to 30-eV range while the bulk distribution has a temperature of only about 0.2 eV. This velocity distribution can result in increases in the plasma line intensity by factors of 50 to 100.

Even more enhancement may occur in the underdense corona of a laser-irradiated target. In this case, the sources of hot electrons are the $2\omega_p$ and SRS-A instabilities occurring near the $n_c/4$ surface. The hot-electron pulses resulting from the intermittent breaking of plasma waves near $n_c/4$ move out into the corona and produce a transient local velocity distribution which can be modeled as a Maxwellian with temperature T_c for the bulk of the electrons, together with a narrow moving pulse of hot electrons moving in the radial direction.

The resultant scattered intensity is evaluated by integrating over the plasma volume, in much the same way as it is done in Ref. 7. The principal contribution to the integral is from the appropriate plasma line. The expression for the fractional scattered power has the usual Thomson scattering angular variation and the usual magnitude, multiplied by a shape factor S which is

$$S = \frac{\left(\frac{E_p}{T_c}\right)^{1/2} \exp\left(-E_p/T_c\right) + \frac{T_c}{E_p}\frac{\bar{\nu}}{\omega}}{\frac{\bar{\nu}}{\omega} + \left(\frac{E_p}{T_c}\right)^{3/2} \exp(-E_p/T_c) + \epsilon\alpha^{3/2}y^2(y-1)\exp\left[-\alpha(y-1)^2\right]} \qquad (1)$$

Here $E_p \equiv \frac{1}{2}m(\omega/k)^2$, $\omega = \omega_o - \omega_s$, $k = |\mathbf{k}_o - \mathbf{k}_s|$, with ω_s and $\mathbf{k}_s$ the frequency and wave vector of the scattered EM wave. The electron-ion collision frequency is denoted by $\bar{\nu}$ and the ratio of the hot-electron density to the cold-electron density by ϵ (assumed small). Also $\alpha = 3T_h/2T_c$ and $y^2 = 2E_pk^2/(3k_r^2T_h)$ with T_h representing the equivalent temperature associated with the central velocity v_h of the moving electron pulse, $3T_h = mv_r^2$; k_r is the radial component of $\mathbf{k}$. Equation (1) is not valid for $\omega_s = \omega_o$ since it has been assumed that $\omega/k \gg (2T_c/m)^{1/2}$.

Major enhancement of the reflected power can occur for ω_s and k_s such that the corresponding radial component of the plasma-wave phase velocity, ω/k_r, falls on the increasing slope portion of the hot-electron pulse, i.e., $y < 1$. If ϵ is large enough, the denominator in Eq. (1) will then become small or negative. The homogeneous-dressed test-particle model is invalid in this limit, but it is certain that very large enhancements will occur. A proper calculation of the scattered intensity will require the solution of a nonlinear problem.

One finds that the two gaps in the spectrum occur in a natural way once ϵ exceeds this critical level. For ω_s near $\omega_o/2$, the plasma-wave phase velocity is high, the resistive terms dominate in Eq. (1) and $S = O(10^{-2})$ for parameters appropriate to the experiments described in Ref. 2 ($T_c = 1$ keV). The resultant scattered intensity is below the experimental detection level by a factor of 10^2–10^3. Again, when ω_s approaches ω_o [but not so close that Eq. (1) is invalid], the phase velocity becomes small enough that the Landau-damping term of the cold electrons dominates and again $S = O(10^{-2})$. These same considerations predict a separated band in the "up-scattering" regions between ω_o and $2\omega_o$ (but not symmetrical to the lower one since k_s will be larger).

If one defines the enhanced radiation intervals as corresponding to regions where the denominator of Eq. (1) vanishes or is negative, it is easy to explore the dependence on various parameters. Using a computer, we have studied the variation of the bands with ϵ, T_c, T_H, and scattering angle θ. An example of these results is shown in Figs. 19.3 and 19.4. In Fig. 19.3, the beginning of "down-scattering" is seen when ϵ exceeds 10^{-4}. The up-scattering sets in when ϵ exceeds 10^{-3}. These results are for $T_c = 1$ keV, $T_H = 18$ keV, and for an internal scattering angle of 90°. Note the broadening of the bands as ϵ increases. Figure 19.4 illustrates shifting and broadening of the bands as the internal scattering angle is varied, for $T_c = 1$ keV, $T_H = 18$ keV, and $\epsilon = 5\times10^{-3}$. We have also noted smaller shifting with variation of T_H, and relatively little with variation of T_c. Recent experimental observations[8] have observed the up-scattered band as well as the down-scattered band, close to where these calculations predict them to be.

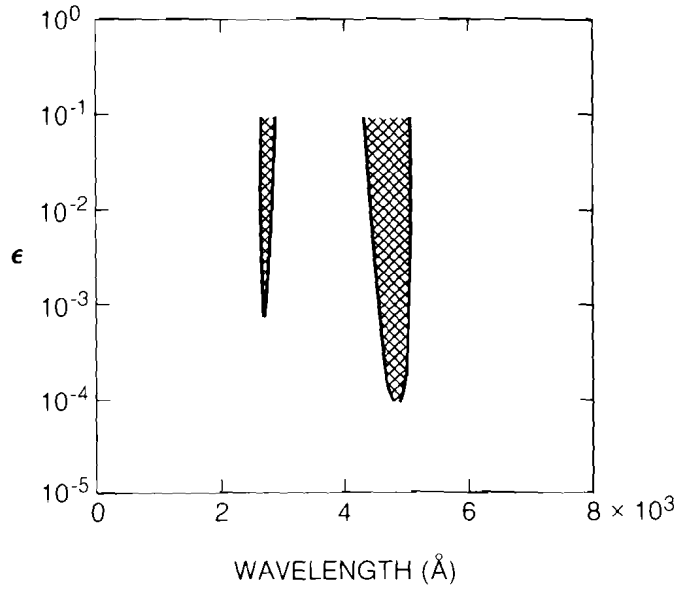

P288

Fig. 19.3
Variation of enhanced Raman-scattering band (hatched area) with ϵ, the ratio of hot-electron density to cold-electron density. This is for scattering at an (internal) angle of 90° with T_h = 18 keV, T_c = 1.0 keV, and incident wavelength λ_0 = 3510 Å.

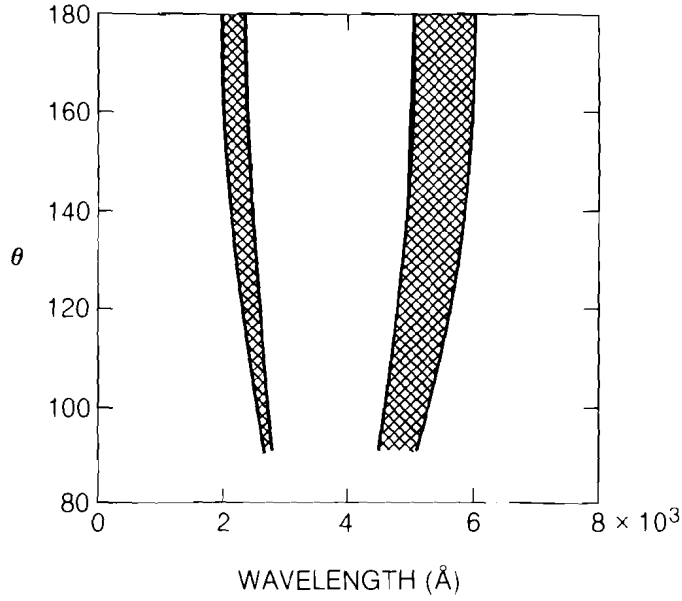

P287

Fig. 19.4
Variation of enhanced Raman-scattering band (hatched area) with (internal) angle of scattering. This is for $\epsilon = 5 \times 10^{-3}$, where ϵ is the ratio of hot-electron to cold-electron density, T_h = 18 keV, T_c = 1.0 keV, and incident wavelength λ_0 = 3510 Å.

Our model also accounts for the other features discussed earlier. The coupling between the onset of the Raman spectrum and the onset of SRS-A is clear since it is presumably the hot electrons from the SRS-A at $n_c/4$ which establish the reversed-slope plasma medium in the subcritical region (i.e., raise the value of ϵ to the critical point). The scintillation clearly arises from the turbulent-pulsed nature of this same source. The azimuthal angular distribution of this ordinary Thomson scattering is relatively gentle compared to the SRS-C. Even at 90°, it is simply $\sin^2\theta$.

In summary, we propose a new model of the Raman spectra observed in laser experiments in inhomogeneous plasma. The scattering is due to ordinary incoherent Thomson scattering (using a greatly enhanced plasma line). The wakes of the incoherent "dressed" electrons are enlarged owing to a reversed-slope velocity distribution in the subcritical region created by bursts of hot electrons moving out from the quarter-critical surface and created there by the breaking of waves resulting from the SRS-A or $2\omega_p$ instabilities. A unique feature of the model is the prediction of appreciable up-scattering, the existence of which has been experimentally observed.

ACKNOWLEDGMENT

This work was supported by the U.S. Department of Energy Office of Inertial Fusion under contract number DE-AC08-80DP40124 and by the Laser Fusion Feasibility Project at the Laboratory for Laser Energetics which has the following sponsors: Empire State Electric Energy Research Corporation, General Electric Company, New York State Energy Research and Development Authority, Northeast Utilities Service Company, Southern California Edison Company, The Standard Oil Company, and University of Rochester. Such support does not imply endorsement of the content by any of the above parties.

REFERENCES

1. D. W. Phillion *et al.*, *Phys. Fluids* **25**, 1434 (1982).
2. K. Tanaka, L. M. Goldman, W. Seka, M. C. Richardson, J. M. Soures, and E. A. Williams, *Phys. Rev. Lett.* **48**, 1179 (1982).
3. R. E. Turner, D. W. Phillion, E. M. Campbell, and K. G. Estabrook, *Phys. Fluids* **26**, 579 (1983).
4. W. Seka, E. A. Williams, R. S. Craxton, L. M. Goldman, R. W. Short, and K. Tanaka, submitted to *Phys. Fluids*.
5. W. Seka (private communication).
6. E. E. Salpeter, *Phys. Rev.* **120**, 1528 (1960).
7. F. Perkins and E. E. Salpeter, *Phys. Rev.* **139**, A55 (1965).
8. L. M. Goldman, W. Seka, K. Tanaka, A. Simon, and R. Short, presented at 14th Annual Anomalous Absorption Conference, Charlottesville, VA, 1984 (unpublished).

2.B Diagnostic Value of Odd-Integer Half-Harmonic Spectra

UV-laser/plasma interaction experiments carried out recently at LLE have significantly extended our understanding of the nonlinear coupling of laser light to the coronal plasma. One of the most important of these parametric processes is the $2\omega_p$ decay instability at the quarter-critical density ($n_c/4$). The signature of this process encompasses a broad spectral band of electromagnetic radiation from $\approx$ 1 eV to several keV. The behavior of structural features in the $\omega_0/2$ and $3\omega_0/2$ spectra reveals a great deal about the internal coronal processes. In particular, some of the features are especially suitable for coronal-electron-temperature diagnostics.

Odd-integer half-harmonic spectra have been observed and reported in the literature since 1970.[1] The connection of these spectra with instabilities occurring in the plasma corona near $n_c/4$ is now clearly established. As such, these spectra can serve as a qualitative diagnostic for the existence of these instabilities, but, in addition, various theoretical predictions[2] have been made for the spectral splitting of the observed, generally double-peaked, spectra. All theories predict a linear relationship between splitting and coronal electron temperature, hence the interest in using these spectra as a coronal-temperature diagnostic. Unfortunately, the spectral splitting generally also depends on geometrical factors such as the angles of incidence and the angles of observation in addition to other effects.[3,4] Since these conditions are usually not very well defined — they typically differ from experiment to experiment — the diagnostic value of these spectra rapidly diminishes as a quantitative analysis requires complex geometrical and other factors to be included.

Recent advances in the understanding of the half-harmonic spectra[5] from spherical UV target-irradiation experiments on the OMEGA laser system have isolated one feature in the half-harmonic spectra which appears to follow a simple relationship between the temperature and its frequency shift from $\omega_0/2$ (ω_0 = irradiation frequency). This shift is independent of detailed geometrical or other effects. However, this feature — a sharp, slightly red-shifted spike — can generally only be seen when viewing the plasma along or close to the density gradient. This particular feature thus represents a convenient diagnostic for the determination of the coronal electron temperature.

The other features in the half-harmonic and the three-halves-harmonic spectra have traditionally been interpreted in various ways although their complex dependences on angles of incidence and angles of observation render them practically useless for temperature diagnostics. In this article we will discuss the various spectral features of the odd-integer half-harmonics, their interpretation, and their diagnostic value for laser plasmas.

A schematic diagram of the irradiation and observation configuration in the $\omega_0/2$ and $3\omega_0/2$ experiments on OMEGA is shown in

Fig. 19.5. One of the six UV beams of OMEGA (λ_L = 351 nm) is shown illuminating the target at an angle of 120° to the axis of the port of observation. If we assume that the plasma is roughly spherical, then the region on the target surface emitting $\omega_0/2$ light into the collection optics is restricted to less than 20° around the direction defined by the target center and the center of the collection optics. This is a result of the fact that the $\omega_0/2$ radiation originates very close to its own critical density; thus, it is refracted strongly and emerges close to the direction of the density gradient in the plasma. This also implies oblique angles of incidence for the other beams at 30° and 60° with respect to the observation port.

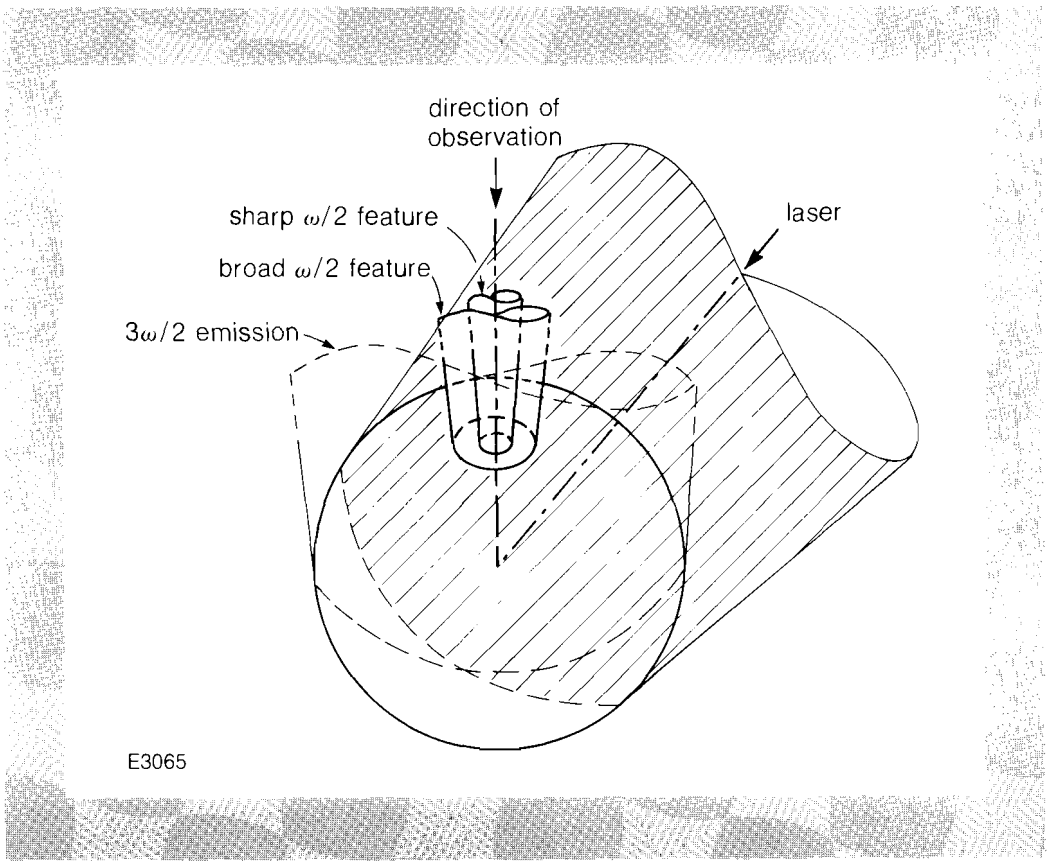

Fig. 19.5
Schematic diagram showing the OMEGA irradiation and observation configuration for the $\omega/2$ and $3\omega/2$ experiments. For clarity, only one laser beam is shown. (Typically, six overlapping beams illuminated the target.) For a particular direction of observation, the sharp $\omega_0/2$ feature is seen only in a small region about the normal to the target surface. The broad $3\omega_0/2$ radiation shows no such preferential direction of emission; thus, the entire hemisphere is visible in this region of the spectrum.

The evolution of half-harmonic spectra with increasing intensity and for different target materials (Z) is shown in Fig. 19.6. We note that only a sharp spike with near resolution-limited width is observed at the lowest intensities. With increasing intensity a clear, additional, spectrally broad, blue-shifted feature appears. A similar, spectrally broad, red-shifted feature of much less intensity also becomes apparent at higher intensities.

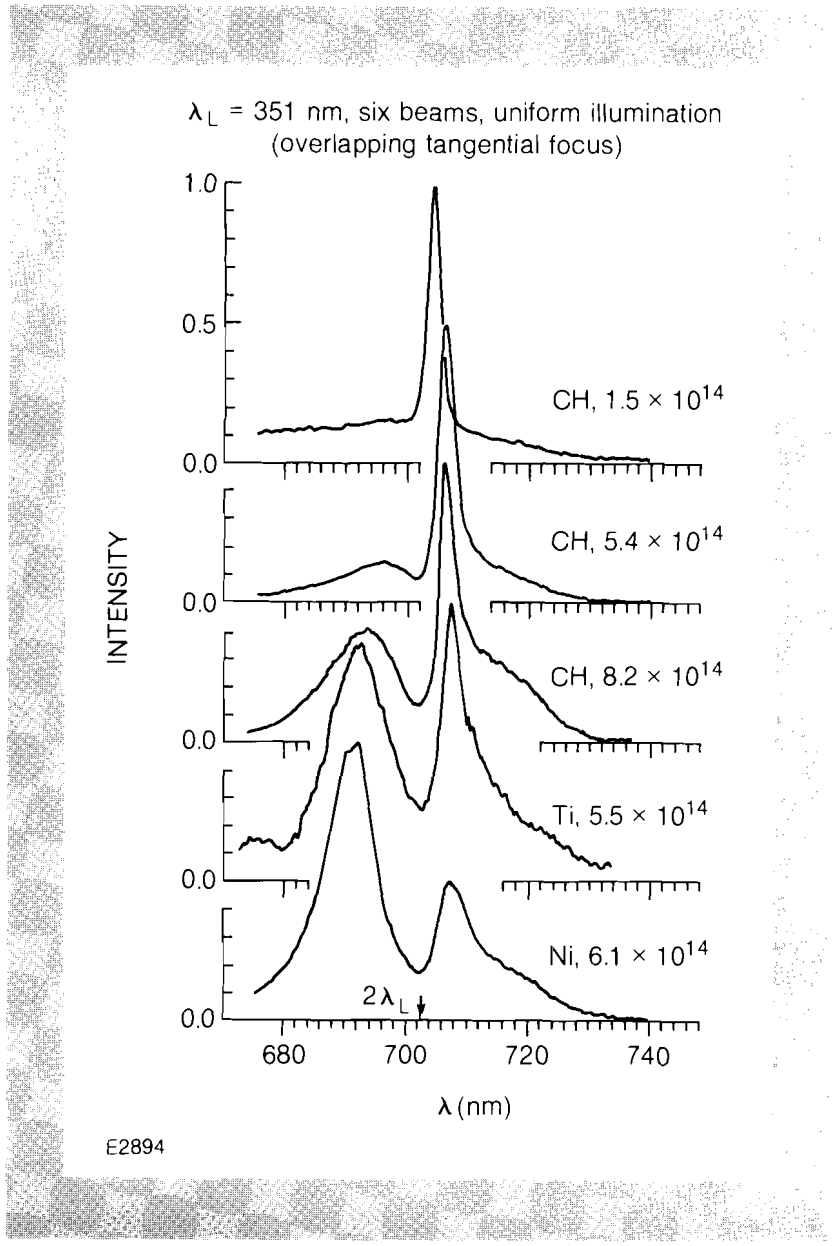

Fig. 19.6
Evolution of $\omega/2$ spectra from uniformly (tangentially) illuminated spherical targets for different irradiation intensities. The sharp, slightly red-shifted peak seen in all spectra can be effectively used for coronal-electron-temperature diagnosis.

In a previous report[5] we have shown a typical spectrum taken in the mid-10^{14} W/cm^2 range and have offered an interpretation in terms of ordinary Raman down-scattering for the sharp feature and in terms of plasmon-photon reconversion (inverse resonance absorption) for the two broad features. Recent theoretical work has strengthened this interpretation of the sharp component, while alternative explanations for the other features now appear more likely, as discussed below.

As the generation of half-harmonic light can involve either the $2\omega_p$-decay instability and/or the absolute stimulated Raman-scattering instability, we must consider the threshold conditions for these processes. Equation (1) shows the threshold relations including effects due to oblique incidence (θ is the internal angle of incidence at $n_c/4$).

$$I_{th}^{2\omega_p} \lambda^2 \left(\frac{L}{\lambda}\right) \frac{1}{T} \approx 7 \times 10^{15} \cos\theta \ (\mathrm{W}\,\mu\mathrm{m}^2/\mathrm{cm}^2\,\mathrm{keV})$$

$$I_{th}^{SRS} \lambda^2 \left(\frac{L}{\lambda}\right)^{4/3} \approx 10^{18} \ (\mathrm{W}\,\mu\mathrm{m}^2/\mathrm{cm}^2). \qquad (1)$$

Here, all intensities are in W/cm^2, the density scale lengths and laser wavelengths are in μm, and T_e is the coronal electron temperature in keV. Typical estimated plasma parameters for our experiments are $T_e \approx 1$ keV, $L \approx 20$-50 μm, $\theta \approx 60°$, and $\lambda_L = 0.35$ μm which lead to threshold intensities of $I_{th}^{SRS} \approx 5\times10^{15}$ W/cm^2 and $I_{th}^{2\omega_p} \approx 1.5\times10^{14}$ W/cm^2. For the range of irradiation intensities in our experiments, $10^{13} \lesssim I \lesssim 2\times10^{15}$ W/cm^2, we are clearly above the $2\omega_p$ instability threshold while we are well below the SRS threshold even after allowance is made for intensity nonuniformities on the target surface. On this basis we reject SRS as a contributing factor to our half-harmonic spectra and will concentrate in the following on the $2\omega_p$ decay instability as the main factor influencing the observed spectra.

In explaining the $\omega_o/2$ spectra it is necessary to refer to a typical $2\omega_p$-decay diagram as shown in Fig. 19.7. Here, the incident photon with frequency ω_o and wave vector k_o decays into two plasmons with $\omega_{p_{1,2}} = \omega_o/2 \pm \Delta\omega$ and $k_{p_{1,2}}$ as shown in the figure where the frequency shift is given by

$$\Delta\omega/\omega_o = 9/4\ \kappa\ (v_T^2 k_o^2/\omega_o^2) \approx 4.4 \cdot 10^{-3}\ \kappa\ T_{e(keV)}$$

and

$$\kappa = \mathbf{k}_{p_1} \cdot \mathbf{k}_o / k_o^2.$$

Fig. 19.7
Wave-vector diagrams for the $2\omega_p$-decay instability and for Raman down-scattering. The $2\omega_p$ diagrams are formed by $\mathbf{k}_o = \mathbf{k}_{p_1} + \mathbf{k}_{p_2}$ while the Raman scattering is given by $\mathbf{k}_s = \mathbf{k}_o - \mathbf{k}_p$. For normal incidence (a) the k-matching conditions for Raman scattering can only be satisfied for $k_s \approx 0$, while for oblique incidence the conditions can only be met for ∇n nearly parallel to $\mathbf{k}_p$.

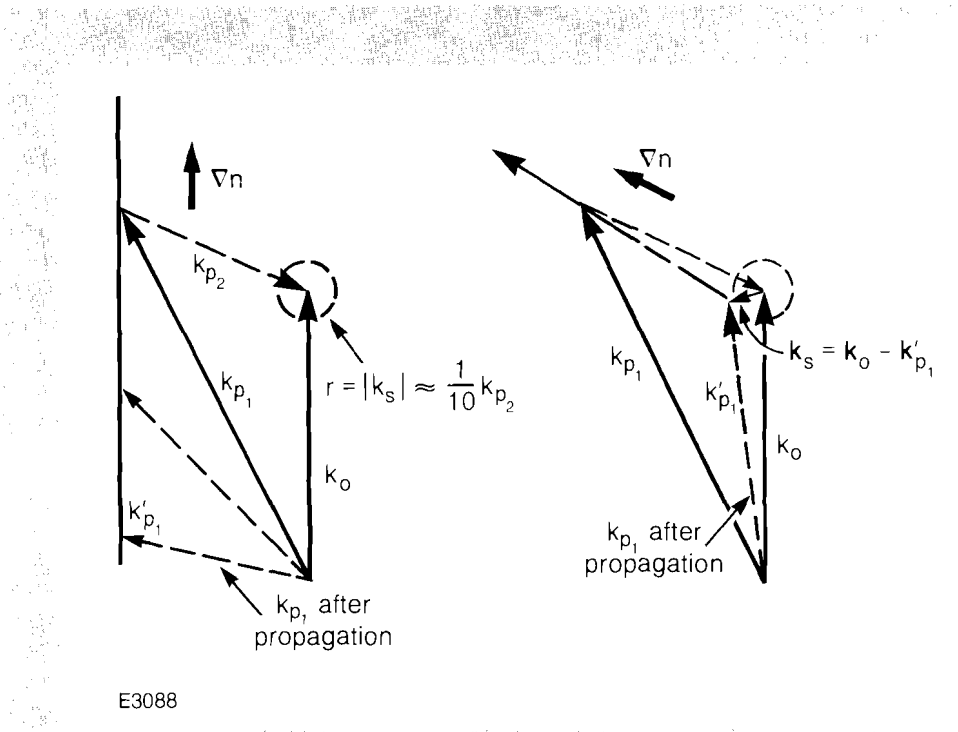

E3088

To generate $\omega_0/2$ light via Raman down-scattering of incident light from plasmons produced by the $2\omega_p$ instability, the Raman frequency and k-matching conditions have to be satisfied, i.e., $\omega_s = \omega_0 - \omega_p$, and $\mathbf{k}_s = \mathbf{k}_0 - \mathbf{k}_p$ (Fig. 19.7). Since the k-vector of the scattered EM wave, k_s, is approximately one-tenth the size of the plasmon k-vector of the same frequency, Raman down-scattering can happen only if one of the plasmon k-vectors is nearly zero or the density gradient is nearly aligned with one of the plasmons, or if the EM wave which scatters off the plasmon is not the same as the incident EM wave giving rise to the $2\omega_p$ decay. The usual theory[6] for the $2\omega_p$ decay instability does not include the mode for which one plasma k-vector is zero or nearly zero. However, recent analysis (theoretical work in progress[7]) indicates that there is indeed such a mode which is similar to, but not identical with, the usual absolute SRS instability.

This decay mode involves two waves — a plasma wave whose k-vector is very nearly equal to the pump-wave vector and a second wave which is a hybrid between an electromagnetic and electrostatic wave of near-zero k-vector. The hybrid wave is expected to radiate light efficiently at a frequency slightly less than $\omega_0/2$. On the basis of k-matching and growth rate considerations, we conclude that the spectrum of this emission is narrow as well as slightly red-shifted. This corresponds to the dominant feature in the spectra shown in Fig. 19.6.

The threshold for this mode is slightly higher than the ordinary $2\omega_p$ threshold, but since this mode is an efficient radiator of $\omega_0/2$ light it may well become visible before any other manifestation of the usual $2\omega_p$-decay instability.

The frequency shift of this narrow, red-shifted $\omega/2$ component is well defined ($\kappa = 1/2$) and given by $\Delta\omega/\omega_0 = 2.2\text{x}10^{-3}\ T_{e\ (\text{keV})}$. The width of this spectral feature is determined by the convolution of the growth rate for the primary decay process and the Raman k-matching conditions. Fortunately, the frequency shift of this mode is not affected by the irradiation or observation geometry. Thus, the sharp and slightly red-shifted half-harmonic spectral feature is a very good temperature diagnostic for the corona. As an application of these conclusions, we have plotted in Fig. 19.8 the intensity dependence of the frequency shift of the narrow, red-shifted component (closed symbols). On the right-hand ordinate the electron temperature scale is shown corresponding to the relationship

$$\Delta\omega/\omega_0 = 2.2 \cdot 10^{-3}\ T_{e\ (\text{keV})}.$$

The temperatures thus deduced are in close agreement with earlier work[8] where certain spectral features of the convective SRS emission were used as a coronal-temperature diagnostic. Hydrocode predictions for these plasmas typically lie 20-50% above measurements reported here. The origin of this discrepancy may lie in the thermal electron transport around the critical density n_c and is currently under active investigation.

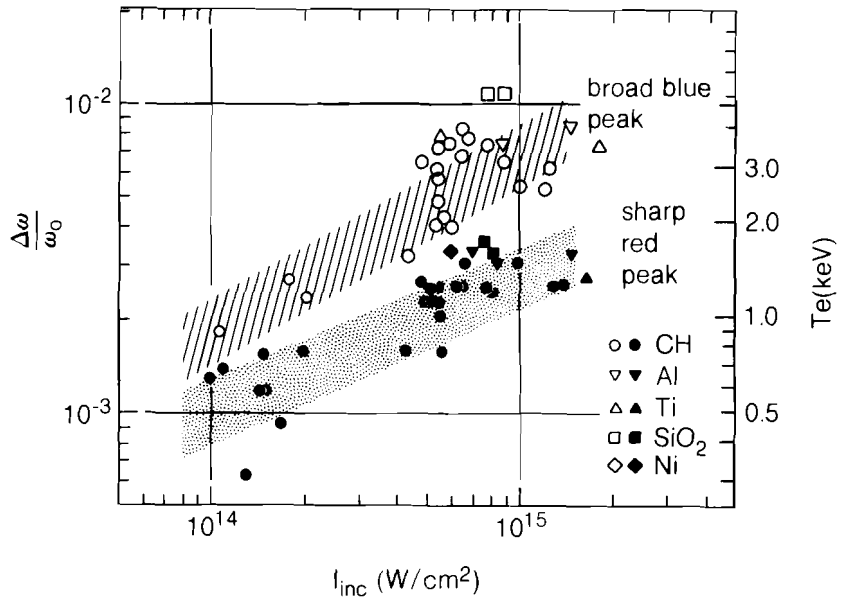

Fig. 19.8
Normalized frequency shifts of $\omega/2$ spectra for uniform (tangential), multi-beam irradiation of spherical targets (λ_L= 351 nm, t_L= 600 ps). The frequency shift of the sharp, red-shifted $\omega/2$ feature is shown in closed symbols. The interpretation of this shift in terms of electron temperature is shown on the right-hand ordinate using the relation $\Delta\omega/\omega_0=2.2\times10^{-3}\ T_e(keV)$. (Note that this temperature scale applies to the solid dots only.) The frequency shift of the broad blue component of the $\omega/2$ spectra is shown in open symbols.

The broad $\omega_0/2$ spectral features seen in Fig. 19.6 can be explained either by inverse resonance absorption (IRA) or Raman down-scattering. Analysis of the former shows that in a one-dimensional (1-D) spherical plasma the resulting spectra should be narrow and their shifts from $\omega_0/2$ should be much smaller than observed. Rippling of the $n_c/4$ density surface could broaden the spectrum, but it still appears that the large observed spectral shifts cannot be explained in this way. Thus, we rule out IRA as the process responsible for the broad features in the $\omega_0/2$ spectra.

Similarly, Raman down-scattering involving incident photons (k_0) and plasmons arising from decays with $k_{p_2} \neq 0$ encounters severe difficulties in satisfying the Raman k-matching conditions. However, Raman down-scattering can generate broad spectral features with the required shifts and widths if we allow the participating EM wave with frequency ω_0 to have a direction other than the incident photons. This process was recently proposed by Turner *et al.*[9] without, however, specifying any further conditions. They could, therefore, not predict any particular spectral shape or shift except for broadly bracketing the spectral range of the $\omega_0/2$ emission. However, we have found a special case of Raman down-scattering[10] which

involves a low frequency ("red") plasmon whose k-vector length is equal to the length of the incident EM wave vector. If we assume the existence of an EM wave with the fundamental frequency and with its wave vector aligned with that of the red plasmon, then the Raman down-scattering conditions are met exactly in the $2\omega_p$-decay region. The result is a blue-shifted $\omega_0/2$ spectral component whose estimated spectral shift and width agree closely with experimental measurements. We note that this is not a general result but one which is a direct consequence of requiring the particular $2\omega_p$ decay with $|k_{p_2}| \approx |k_0|$.

The theoretical analysis of this Raman down-scattering process further shows that the blue-shift of this component bears a nearly constant relationship to the frequency shift of the sharp red component, independent of geometry and intensity. That is, the two shifts differ by approximately a factor of 2. This conclusion also agrees closely with our observations, as is borne out in the intensity scaling of the frequency shifts of the two half-harmonic spectral features (open and closed symbols in Fig. 19.8). In this context it is also interesting to note that the data points for the blue peak set in at higher irradiation intensities than those for the red peak. This is also seen in Fig. 19.6, and finds its explanation in the higher thresholds for the $2\omega_p$ decays involving the long plasmon k-vectors necessary for the blue Raman down-scattering component.

Another consequence of this model is that the spectrally broad blue component is emitted into a much wider cone around the direction of the density gradient than the sharp red spike. This is due to the lengths of the scattered k-vectors k_s, which are essentially zero for the sharp red-shifted spike (the emission originates at its critical density) while for the spectrally broad blue-shifted component they are $|k_s| \approx 0.2|k_0|$. That is, the emission originates from a region with considerably less than its critical density. Viewed from outside the plasma, the cone angle for this emission can be estimated to be

$$\theta \approx \sin^{-1}\left(\frac{0.2 \times 0.87}{0.5}\right) \approx 20°.$$

This agrees closely with observations made here in our experiments as well as elsewhere,[9] in which the sharp, red-shifted component appears to emanate from a narrow coronal region. This region is centered about the normal to the target surface that passes through the observation point.

The origin of the EM waves (k_0', ω_0) which give rise to the blue-shifted Raman component may in our experiments come from one of the other six beams illuminating the target. In flat-target experiments as reported in Ref. 9, the scattered fundamental radiation could come from a rippled critical-density surface or from filamentation which had to be invoked for the interpretation of data obtained in such experiments.[2,11] Turner *et al.*[9] have suggested stimulated Brillouin scattering as an alternative source for the scattered light. We cannot rule out this source in our experiments although we have never observed evidence for stimulated Brillouin side-scattering.

The low-intensity, broad, red-shifted component in the half-harmonic spectra (Fig. 19.6) can be explained in a manner similar to the explanation for the blue component. Here, however, propagation of the high-frequency (blue) plasmon in the density gradient is required. Regarding spectral shifts and widths, the same arguments apply as delineated above, making this red feature symmetrical to the blue feature in all aspects except its intensity. The latter is expected to be lower because the blue plasmon must propagate approximately 1 μm in the density gradient before reaching the Raman k-matching point.

In short, the half-harmonic spectra now appear to be reasonably well understood, with one feature exhibiting a red-shift (sharp red spike) which is simply related to the coronal electron temperature. However, this feature is generally only observed when viewing the plasma close to the target normal (along the density gradient). The other prominent feature of the $\omega_0/2$ spectra is a broad blue component which is more easily observed (within $\approx 20°$ of the target normal) and whose blue-shift is roughly twice the frequency shift of the sharp red component. Although this proportionality is somewhat dependent on irradiation intensity and geometry, it is sufficiently close to make this spectral feature an alternate (though less desirable) candidate for coronal-temperature diagnostics. The third and much weaker component now appears to be understood the same way as the broad blue peak, but because of its weakness its diagnostic value is of minor importance.

The coronal-temperature diagnostic most frequently reported in the literature uses the splitting of the 3/2-harmonic spectra. The theories usually applied[2] predict symmetrically split spectra for normal incidence. All $3\omega_0/2$ light generated in the backward direction is red shifted, while the forward component is blue shifted with the shifts depending strongly on the angle of observation. For overdense targets this translates into symmetrically split spectra in the backscatter direction, but the detailed predictions of the 1-D theory have never been verified experimentally. Recent spectra taken with thin targets[3] have, however, shown interesting angular dependence of the emitted $3\omega_0/2$ spectra which could be understood in terms of filamentation of the incident laser light in the plasma. Since truly 1-D plasmas are extremely difficult to produce, most of the experimental spectra probably suffer from various two-dimensional (2-D) effects which can wash out the expected angular dependence of the spectral splitting. Under those conditions the average splitting is extremely difficult to predict, thereby reducing significantly the value of the 3/2-harmonic spectra as a coronal-electron-temperature diagnostic. Typically, the temperatures deduced from applying existing theories without geometrical correction factors lie two to three times above those which would be obtained from the half-harmonic spectra discussed above.

Typical 3/2-harmonic spectra obtained on OMEGA six-beam experiments are shown in Fig. 19.9 for nonuniform illumination of the targets. The poor reproducibility and irregularity of these spectra

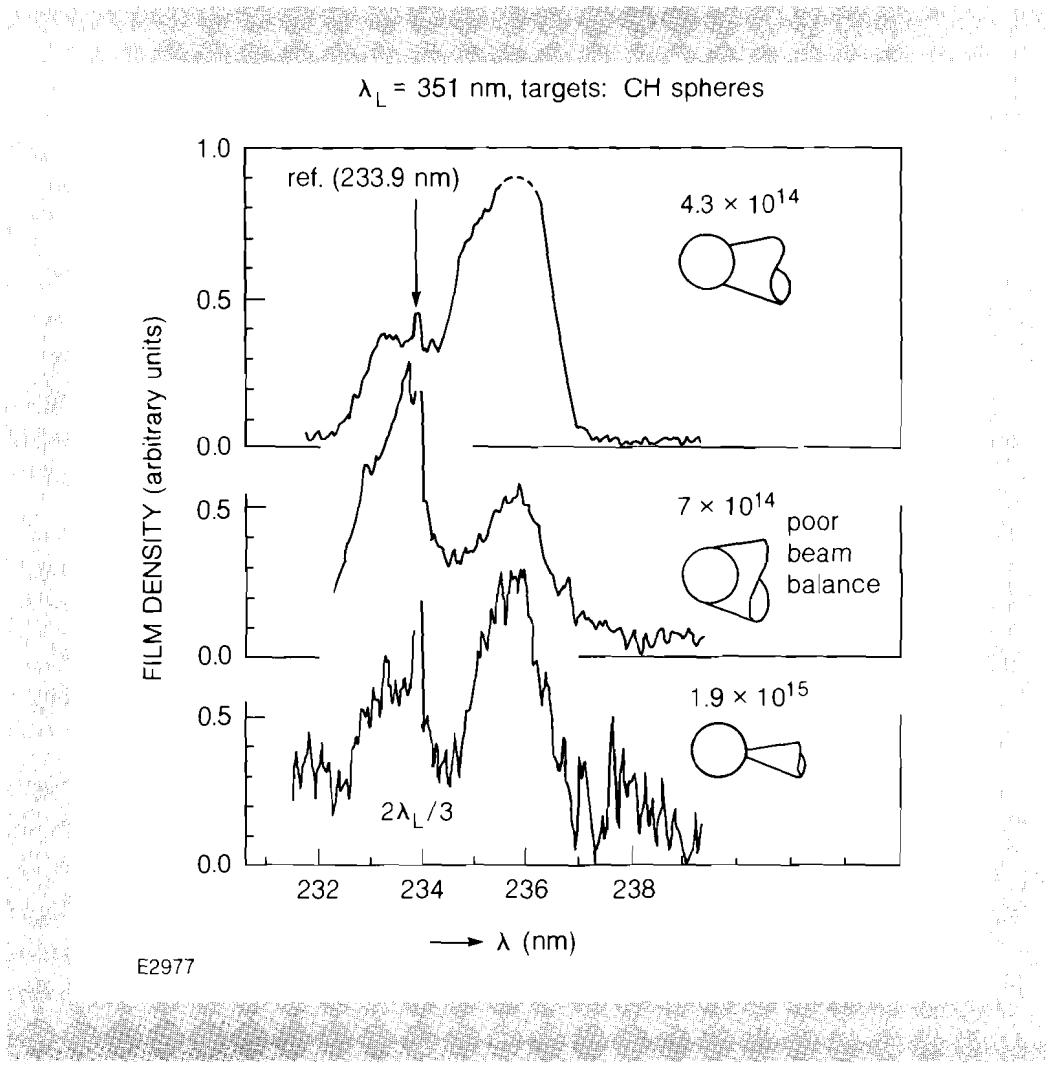

Fig. 19.9
Three-halves-harmonic spectra obtained on the six-UV-beam OMEGA system for nonuniform illumination of targets (focusing as indicated in the inserts). We note the strongly changing spectral features under these conditions which reflect the dependence of these spectra on irradiation and observation configuration.

underline the conclusions drawn above — that the 3/2-harmonic spectra are very sensitive to geometrical factors. The intensity dependence of the spectral splitting of the 3/2- and 1/2-harmonic spectra is shown in Fig. 19.10. For simplicity we have drawn half the spectral splitting of the $3\omega_0/2$ spectra along with the normalized frequency shift of the sharp red spike of the $\omega_0/2$ spectra. If the two processes were to sample the same plasmons, the two sets of data would lie on top of each other. It is evident from this figure that the intensity scaling is different for the two sets of data. Thus, we conclude that the 3/2-harmonic spectra hardly reflect any particular feature of the plasmon spectra produced by the $2\omega_p$-decay instability. The usefulness of the 3/2-harmonic spectra is therefore reduced to a qualitative answer to the questions of the existence of the $2\omega_p$-decay instability in the plasma.

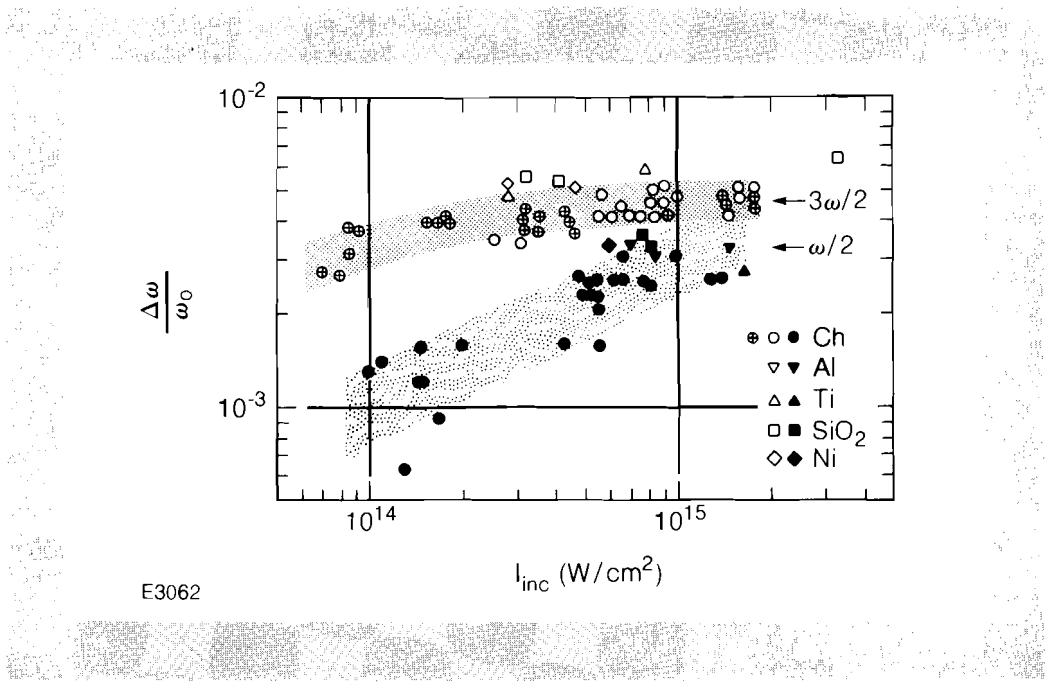

Fig. 19.10
Normalized frequency shift of the sharp red feature of the $\omega/2$ spectra and half of the spectral splitting of the $3\omega/2$ emission under uniform six-beam illumination. For the $3\omega/2$-data results from IR (1.05 μm) and UV (0.35 μm, o and other open symbols) irradiation, experiments are plotted together as the results are virtually indistinguishable. If the two harmonic generation processes were to sample the same plasmons, the two sets of data would lie on top of each other.

ACKNOWLEDGMENT

This work was supported by the U.S. Department of Energy Office of Inertial Fusion under contract number DE-AC08-80DP40124 and by the Laser Fusion Feasibility Project at the Laboratory for Laser Energetics which has the following sponsors: Empire State Electric Energy Research Corporation, General Electric Company, New York State Energy Research and Development Authority, Northeast Utilities Service Company, Southern California Edison Company, The Standard Oil Company, and University of Rochester. Such support does not imply endorsement of the content by any of the above parties.

REFERENCES

1. A. Caruso *et al.*, *Phys. Lett.* **33A**, 29 (1970).
2. A. I. Avrov *et al.*, *Sov. Phys. JETP* **45**, 507 (1977); V. Yu. Bychenkov, V. P. Silin, and V. T. Tikhonchuk, *Sov. J. Plasma Phys.* **3**, 730 (1977); A. N. Starodub and M. V. Filippov, *Sov. J. Plasma Phys.* **5**, 610 (1979); H. C. Barr, Rutherford Laboratory Annual Report No. RL-79-036 (1979), Sec. 8.3.3 (unpublished); V. V. Aleksandrov *et al.*, *JETP Lett.* **37**, 81 (1983); V. Yu. Bychenkov, A. A. Zozulja, V. P. Silin, and V. T. Tichonchuk, *Beitr. Plasmaphys.* **23**, 331 (1983).
3. R. W. Short, W. Seka, K. Tanaka, and E. A. Williams, *Phys. Rev. Lett.* **52**, 1496 (1984).
4. L. V. Powers and R. J. Schroeder, *Phys. Rev.* **A29**, 2298 (1984).
5. LLE Review **14**, 18 (1983).

6. A. Simon, R. W. Short, E. A. Williams, and T. Dewandre, *Phys. Fluids* **26**, 3107 (1983).

7. B. B. Afeyan (private communication).

8. W. Seka, E. A. Williams, R. S. Craxton, L. M. Goldman, R. W. Short, and K. Tanaka, *Phys. Fluids* (to be published August, 1984); see also LLE Review **11**, 3 (1982); **17**, 18 (1983).

9. R. E. Turner, D. W. Phillion, B. F. Lasinski, and E. M. Campbell, *Phys. Fluids* **27**, 511 (1984).

10. T. W. Johnston (private communication).

11. H. Figueroa, C. Joshi, H. Azechi, N. A. Ebrahim, and K. Estabrook, *Phys. Fluids* (to be published, 1984).

2.C Illumination-Uniformity Considerations for Direct-Drive Fusion Reactors

Several authors have studied the illumination uniformity attainable with overlapped multiple laser beams on a spherical target.[1-4] Skupsky and Lee[5] were the first to decompose the illumination pattern on a sphere in terms of spherical harmonics, in order to analyze the nonuniformity pattern according to its spatial wavelengths. The wavelength information is important because a short-wavelength nonuniformity might be smoothed by thermal conduction within the pellet. Reference 5 includes a nonuniformity analysis of the existing 24-beam OMEGA facility at LLE, as well as a 32-beam, f/20 system. It was shown that the 32-beam system could achieve the required uniformity of less than 1% rms in a limited focal region while occupying only 0.5% of the reactor solid angle. Modest thermal smoothing extended the useful region of the 32-beam geometry to include the entire focal region of interest for direct-drive laser fusion. We have extended the work in Ref. 5 to include 20, 32, 60, and 96 beams evaluated for 2% and 8% solid-angle fractions in the reactor. This activity is part of a preconceptual reactor design named SIRIUS conducted in collaboration with the Nuclear Engineering Department of the University of Wisconsin.[6]

The disposition of the final optical elements in the reactor chamber is determined by three related variables: (1) the size of the laser aperture, (2) the distance from the target, and (3) the solid angle subtended by the beams. The laser aperture is determined by the total laser energy and the laser-induced damage threshold of the last focusing optic. The final optic spacing from the pellet determines the reaction-product loading on the optic, and the solid-angle fraction has an impact on the performance of the reactor-blanket. Any two of these variables determine the third. We have chosen to estimate both the laser aperture and an acceptable total solid angle, thereby fixing the final optic distance without regard to the reaction-product loading. It should be noted that holding the solid-angle fraction constant as

the number of beams, N, is varied does not change the distance of the final optic from the pellet. This allows us to study the illumination uniformity effects of N beams without changing this basic design parameter.

The total aperture of the laser driver is determined by the laser energy and the optical damage threshold of the reflective coating on the last focusing optic. For this study we have used values of 2 mJ for the driver energy (at 248 nm) and a damage threshold of 5.0 J/cm^2. When the damage threshold value is combined with the assumed geometrical fill factor (0.7) and a safety factor for ripples on the beam (0.5), the overall threshold is 1.75 J/cm^2. This dictates a total laser aperture of 144 m^2. This aperture is independent of the system configuration, whether direct or indirect drive. The corresponding single-beam apertures for 20, 32, 60, and 96 beams are given in Table 19.I.

NUMBER OF BEAMS	20	32	60	96
beam aperture (m)	2.7	2.1	1.6	1.2
f-number for 2% solid angle fraction	7.9	10.0	13.7	17.3
f-number for 8% solid angle fraction	3.9	5.0	6.8	8.6

- Final optic spacing from pellet
  2% solid angle fraction - 21.3 m
  8% solid angle fraction - 10.6 m

A105

Table 19.I
SIRIUS parameters.

The second variable in the system configuration is the solid-angle fraction the driver occupies in the reactor. This is related to the number of beams and the f-number of the beams by the following expression:

$$\frac{\Delta\Omega}{4\pi} = \frac{N}{2}\left(1 - \frac{2f}{(4f^2+1)^{1/2}}\right). \qquad (1)$$

For the SIRIUS study we are evaluating 2% and 8% solid-angle fractions for the laser beams. The appropriate f-numbers for each of the beam configurations has been calculated using Eq. 1 and is given in Table 19.I. This f-number and the individual beam aperture give the spacing of the final optic from the pellet. The 2% solid-angle fraction places the final optic 21.3 m from the pellet, and the 8% solid-angle fraction has a 10.6-m spacing. This approach allows an evaluation of the effect of dividing the total laser aperture into N beams while maintaining a constant solid-angle fraction in the reactor. The cost scaling of the driver with N is not currently well understood and is beyond the scope of this study. Here we attempt to show the uniformity scaling with N, so that future work can balance the cost scaling of a driver against the uniformity scaling.

The formalism used in this work has been described in detail in Ref. 5 and is briefly reviewed here. The irradiation pattern on the sphere is decomposed into spherical harmonics where the standard deviation of a mode amplitude is given by

$$\sigma_\ell = \left|\frac{E_\ell}{E_0}\right| \left[(2\ell+1) \sum_{k,k'} P_\ell(\Omega_k \cdot \Omega_{k'}) \frac{W_k W_{k'}}{W_T^2}\right]^{1/2} \quad (2)$$

The single-beam factor $|E_\ell/E_0|$ is determined by the focus position, f-number, beam profile, and assumed target conditions. This single-beam factor is evaluated by tracing rays through the pellet plasma shown in Figure 19.11. The remainder of Eq. 2 is the geometrical factor which is determined by the number and orientation of the beams (Ω_k) and the beam energies (W_k). The sum is over all beams; $W_T = \Sigma W_k$ and P_ℓ is a Legendre polynomial. The rms standard deviation of all modes is defined as

$$\sigma_{rms} = \left(\sum_{\ell \neq 0} \sigma_\ell^2\right)^{1/2}. \quad (3)$$

We have calculated the nonuniformity, in terms of σ_{rms}, for a variety of conditions. Earlier work[5] indicated that a quadratic beam-intensity profile of the following form produced good uniformity

$$I = I_0 \left(1 - \frac{r^2}{r_0^2}\right) \quad (4)$$

where r_0 is the pellet radius.

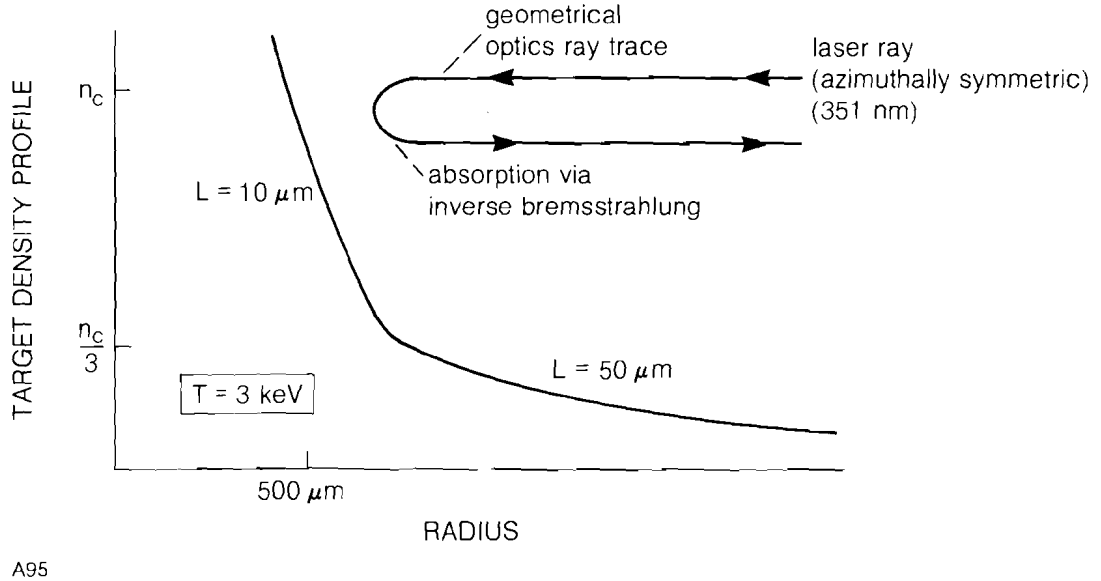

Fig. 19.11
Target conditions for single-beam factor calculations.

The σ_{rms} for a 2% solid-angle fraction geometry is plotted in Fig. 19.12 for 20, 32, 60, and 96 beams as a function of a focus ratio. The focus ratio is defined as

$$\text{focus ratio} = \frac{F}{2fr_o} . \tag{5}$$

F is the position (in mm) of the geometrical best focus beyond the pellet center, r_o is the pellet radius (in mm), and f is the beam f-number. A focus ratio of 1 corresponds to tangential focus where the beam aperture ($2R_o$) illuminates a hemisphere of the pellet ($2r_o$).

The maximum tolerable nonuniformity is generally assumed to be around 1% rms for targets with a convergence ratio (ratio of initial to compressed fuel radius) of less than ~ 20. Such uniformity must be maintained during the entire time of laser irradiation. Figure 19.12 shows that rms nonuniformities of less than 1% can be achieved over a specific range of focus ratios. The focus ratio changes during the implosion as the target is compressed [i.e., r_o in Eq. (5) becomes smaller]. Reactor target simulations indicate that the target can be driven to ~ 60% of its initial radius by the time that the laser pulse attains maximum intensity. Therefore, if the initial focus is tangential, that is, focus ratio = 1, then the focus ratio will increase during target compression to a value of 1.67 at peak pulse intensity. To obtain high uniformity over this range, Fig. 19.12 shows that one option for direct-drive laser fusion is to use 60 or more beams.

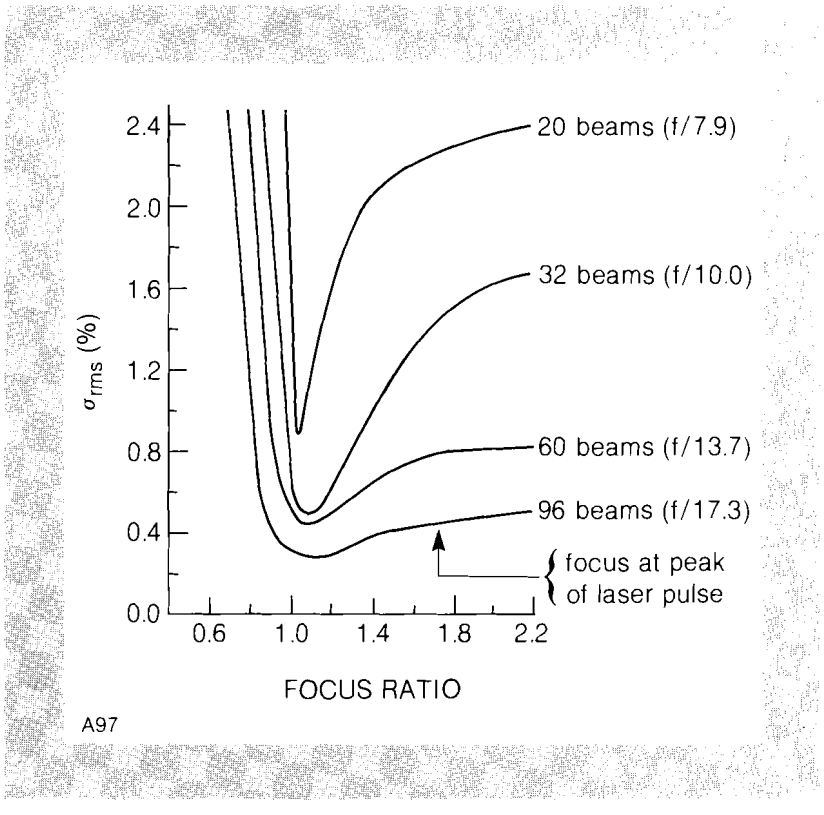

Fig. 19.12
Nonuniformity of laser-energy deposition for 2% solid-angle fraction.

High drive uniformity can also be obtained with few beams (~ 32) if thermal smoothing within the target is found to be effective. This is illustrated in Fig. 19.13 for a 32-beam system at f/20. The dotted curve represents the attenuation of nonuniformities due to moderate thermal smoothing and shows that less than 0.5% rms nonuniformity is maintained over the entire focal region of interest. For this calculation it was assumed that the fractional separation distance between the critical and ablation surfaces ($\Delta R/R$) was 0.1, which is characteristic of short-wavelength laser irradiation during the time of significant laser-energy deposition.

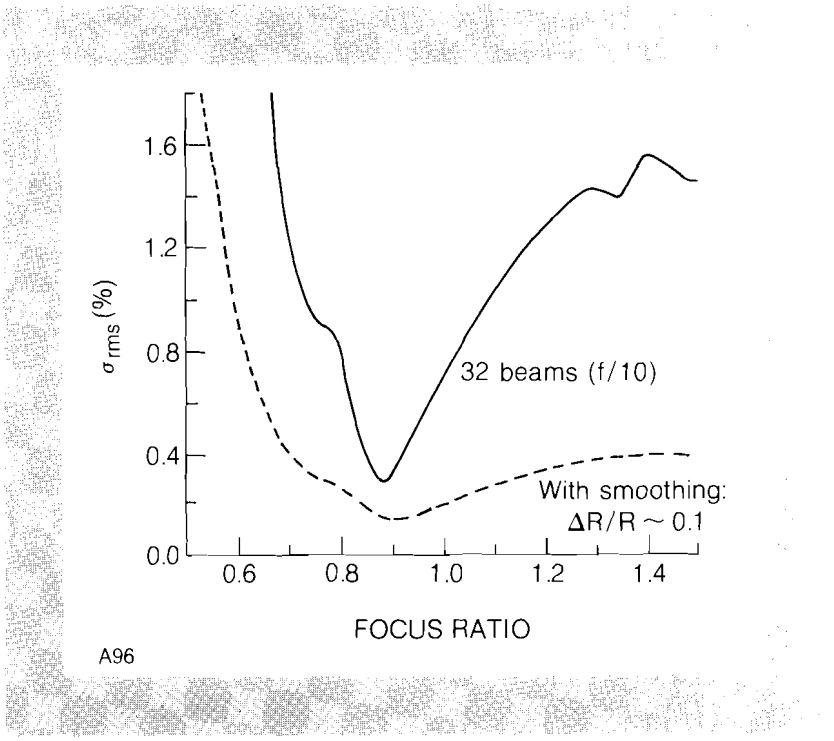

Fig. 19.13
The effect of moderate thermal smoothing on the 32-beam nonuniformity.

The effect of changing the total solid angle subtended by the beams has been studied and is displayed in Fig. 19.14. There is a small improvement in uniformity for the 32-beam system in going from 2% to 8% of 4π, resulting from the change between f/10 and f/5 optics. Changes above ~ f/10 have a negligible effect on uniformity as seen in the 96-beam case which represents a change from f/9 to f/17, because the laser rays are already effectively parallel.

The effects of beam-to-beam energy imbalance were also studied. These create predominantly long-wavelength nonuniformities ($\ell \lesssim 4$). The sensitivity to energy imbalance is reduced as the number of beams is increased. Figure 19.15 shows the effect of a 2.8% rms random variation for the 60- and 96-beam geometries. With this imbalance, typical of the value achieved on OMEGA, the irradiation nonuniformity still stayed below 1% rms.

These calculations used an idealized laser-beam profile. Realistic radial-beam profiles might not be as smooth as the quadratic form used here due to, for example, diffraction effects. The effect of small-

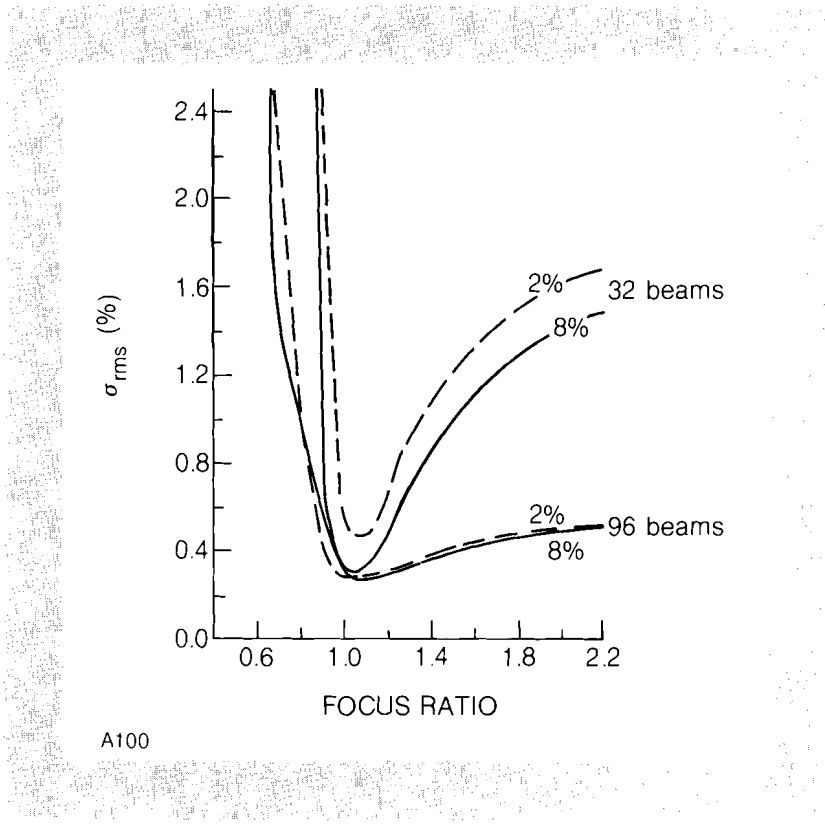

Fig. 19.14
Uniformity for increased solid-angle fraction.

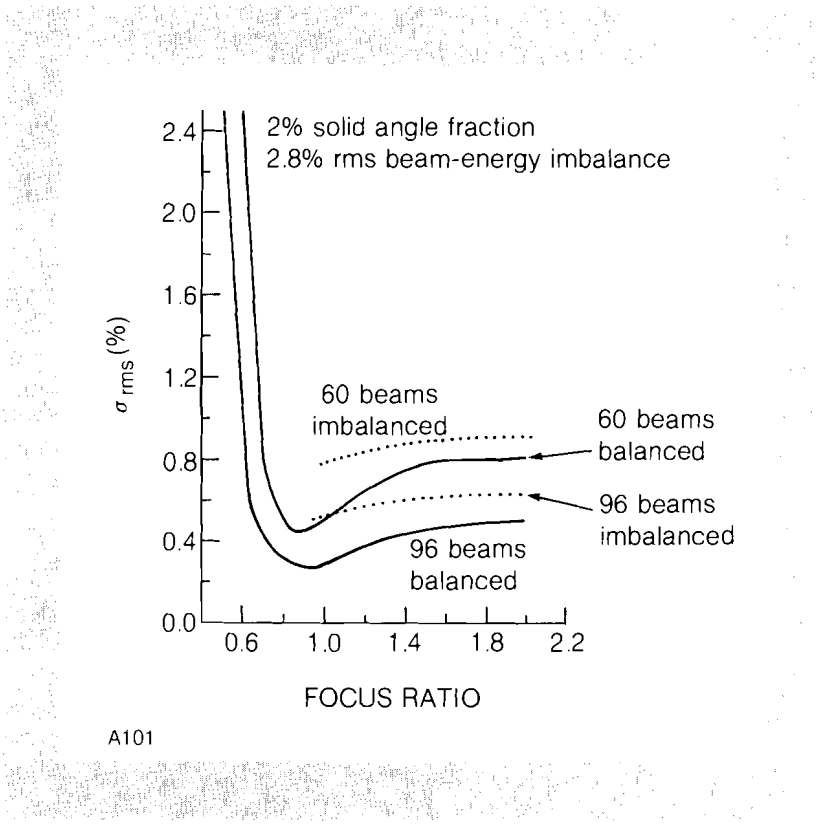

Fig. 19.15
Uniformity with energy imbalance.

scale variations on the radial-beam shape has been examined using a modulated quadratic profile of the form:

$$I = I_0 \left(1 - \frac{r^2}{r_0^2}\right) [1+\epsilon \cos (\pi M r/r_0)]$$

where ϵ and M are parameters controlling the magnitude and wavelength of the modulations. Physically, M/2 can correspond to the number of diffraction rings. Figures 19.16 and 19.17 are nonuniformity calculations for 32 and 96 beams with a 2% solid-angle fraction. To demonstrate the effect of only a small amount of smoothing, we multiply each σ_ℓ by the factor $\exp(-\ell/20)$, corresponding to $\Delta R/R = 0.05$. Note the rapid drop in nonuniformity for $M > 8$. Additional simulations have shown the magnitude of the nonuniformities scales approximately linearly with ϵ. These results suggest that laser systems for future fusion reactors should be designed with not less than ~4 diffraction rings and/or an intensity variation $\Delta I/I$ considerably less than the 20% used here, both of which are within the limits of present-day technology (see Fig. 19.18). In addition, the effect of the intensity modulation is greatly reduced as the number of beams is increased.

Fig. 19.16
32-beam modulated profile.

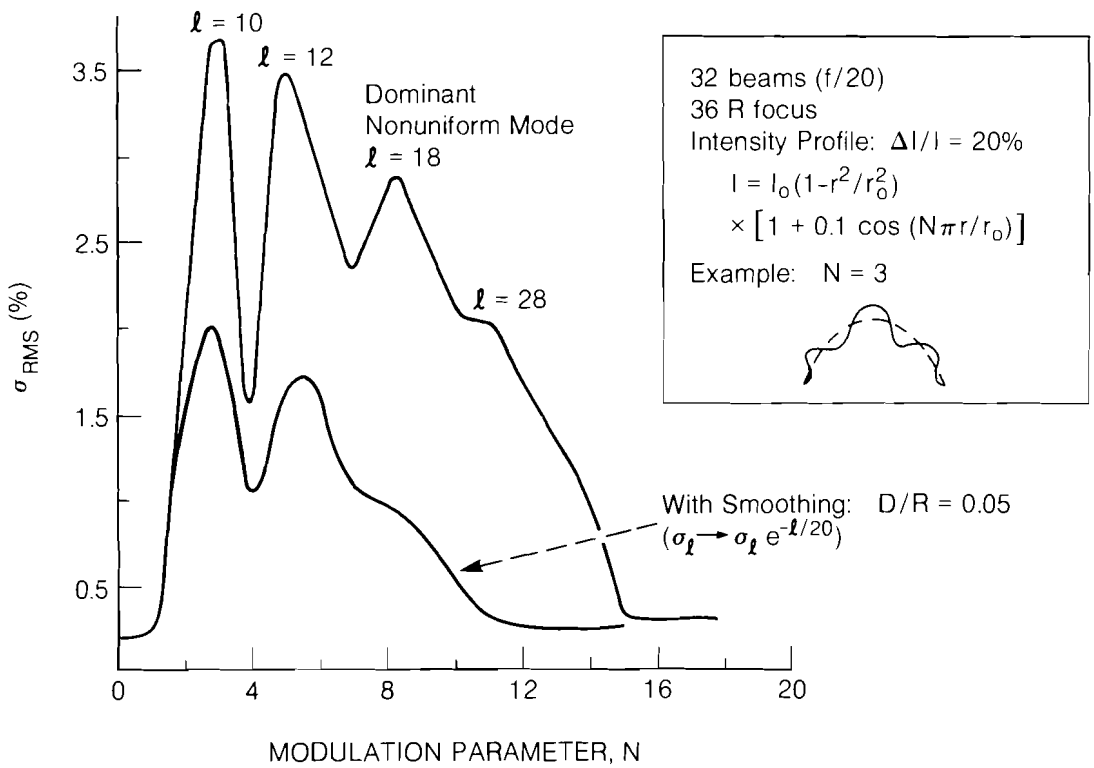

TC1399

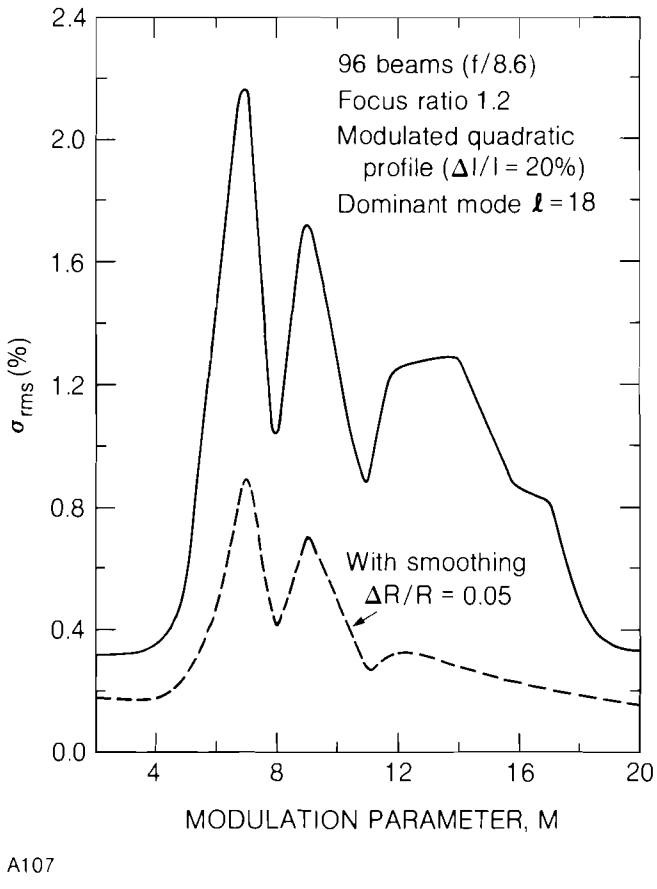

Fig. 19.17
96-beam modulated profile.

We routinely measure the intensity distribution of LLE lasers at the plane of the target. These photographs are referred to as equivalent-target-plane or ETP photos. Generally these are digitized, and an azimuthally averaged plot is generated. One such plot is shown in Figure 19.18. This profile was compared with the quadratic and flat-top profiles for a 96-beam geometry in Figure 19.19. This current profile approaches both idealized profiles if the focus ratio is around 2.0, because the central portions of all three profiles are similar.

The extension of the spherical harmonic analysis of symmetric illumination to 96 beams has shown that the sensitivity of the pellet illumination uniformity to various perturbations, such as energy imbalance and intensity modulation, is greatly diminished when a large number of beams are used. Using greater than ~ 60 beams (with the total beam solid angle at ~ 2%) provides one possible option for the direct-drive approach to laser fusion. If thermal smoothing is found to be an effective mechanism for reducing nonuniformities, then fewer beams, around 32, could provide adequate illumination uniformity.

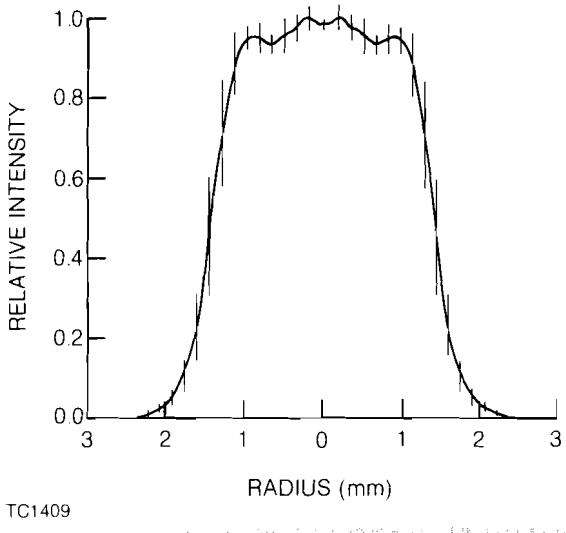

Fig. 19.18
Current beam profile from LLE laser system.

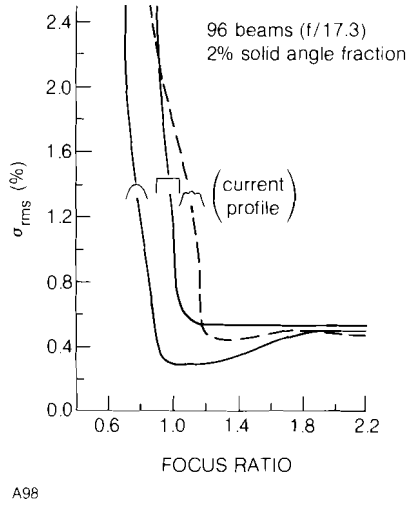

Fig. 19.19
Uniformity depends on laser beam profile.

ACKNOWLEDGMENT

This work was supported by the U.S. Department of Energy Office of Inertial Fusion under contract number DE-AC08-80DP40124 and by the Laser Fusion Feasibility Project at the Laboratory for Laser Energetics which has the following sponsors: Empire State Electric Energy Research Corporation, General Electric Company, New York State Energy Research and Development Authority, Northeast Utilities Service Company, Southern California Edison Company, The Standard Oil Company, and University of Rochester. Such support does not imply endorsement of the content by any of the above parties.

REFERENCES

1. J. E. Howard, "Uniformity of Illumination of Spherical Laser-Fusion Targets," *Appl. Opt.* **16**, 2764 (1977).
2. J. B. Trenholme, "Target Illumination of Shiva," Laser Program Annual Report - 1974, LLNL Report UCRL-50021-74, Livermore, CA.
3. J. B. Trenholme and E. J. Goodwin, "Theory and Design Analysis," Laser Program Annual Report - 1979, LLNL Report UCRL-50021-79, Livermore, CA.
4. J. B. Trenholme, "Nova Target Illumination Studies," Laser Program Annual Report - 1980, LLNL Report UCRL-50021-80, Livermore, CA.
5. S. Skupsky and K. Lee, *J. Appl. Phys.* **54**, 3662 (1983).
6. "Preliminary Conceptual Design of SIRIUS, A Symmetric Illumination, Direct Drive Laser-Fusion Reactor," University of Wisconsin Report UWFDM-568 and LLE Report 152.
7. S. E. Bodner, *J. Fusion Energy* **1**, 221 (1981).
8. R. Kingslake, *Lens Design Fundamentals* (Academic Press, 1978).
9. Copyright by Genesee Computer Center Inc., Rochester, New York.

Section 3
ADVANCED TECHNOLOGY DEVELOPMENTS

3.A Subpicosecond Electro-Optic Sampling Using Coplanar Strip Transmission Lines

The development of new ultrafast electrical devices has stimulated considerable effort to find suitable ways to characterize them. Measurement systems must have both subpicosecond resolution and microvolt sensitivity.

Several systems that meet these requirements have been assembled and tested at LLE. Exploiting the speed of the electro-optic effect and high-repetition-rate subpicosecond laser technology, these systems exhibit response times faster than 1 ps and sensitivities of 50–100 μV. In this section, we describe our newest high-speed electro-optic measurement system. This system avoids certain physical limitations of earlier systems.

Detailed descriptions of our earlier ultrafast electro-optic sampling system have been published.[1,2] In this system the electrical test signal is generated when 100-fs pulses from a colliding-pulse mode-locked laser trigger a Cr:GaAs photoconductive switch. A second beam of pulses is used to probe the birefringence induced by the electrical pulses as they propagate down a transmission line built on $LiTaO_3$. With signal averaging, submillivolt signals are recovered. The temporal response, which was previously limited by the transit time of the optical pulses across the electrode width (i.e., a few ps), was improved by working in a velocity-matching geometry, which is obtained for a particular angle of incidence of the probe beam on the electro-optic crystal. With the proper crystal orientation, a rise time of

500 fs was obtained, limited in part by the transit time of the electrical signal across the beam waist. In this scheme strong dispersion effects occur when the wavelength of the electromagnetic signal is of the order of the cross-sectional dimensions of the transmission line. In order to decrease the amount of dispersion, the transmission-line thickness was decreased to 100 μm. In order to improve the temporal response of the sampler in this configuration, the balanced transmission-line dimensions have to be decreased to the 10-μm range, a severe mechanical constraint.

In order to alleviate the stringent mechanical requirement on substrate thickness, we have used coplanar striplines which do not have the physical limitations of the previous transmission-line geometry.

Coplanar-waveguide (CPW) and coplanar-strip (CPS) transmission lines have been used frequently in microwave integrated-circuit applications.[3] They are generally more easily fabricated than balanced microstrip lines because both the signal and ground lines may be made in the same process step on the same surface of a relatively thick substrate. An even greater advantage, however, is that the electrode dimensions can be reduced to the order of a few microns if the electrodes are fabricated photolithographically. The electrode separation, which is analogous to the substrate thickness in the balanced microstrip geometry, can be made one to two orders of magnitude smaller than is possible for the balanced strip line. This implies that dispersion effects can be reduced even further than was previously possible.

Coplanar geometries have been theoretically characterized to a much lesser extent than have microstrip configurations.[4–7] Calculations available at the present time indicate that coplanar strip transmission lines with dimensions of tens of microns should have frequency cut-offs near 1 THz.[8] Calculations for the frequency dependence of the effective dielectric constant that were originally performed at lower frequencies by Knorr and Kuchler[7] are currently being extended into the terahertz range. These calculations are needed to predict the cut-off frequency for the coplanar strip lines of interest.

Experiment

The experimental arrangement is identical to that of Ref. 1 with the exception of the geometry of the transmission line. A schematic of the coplanar strip transmission line, including the propagating electrical signal and the orientation of the probe laser beam, is shown in Fig. 19.20.

The Cr:GaAs and $LiTaO_3$ crystals were mounted side by side on a glass plate and were subsequently ground and polished together to a thickness of 500 μm in order to present a uniformly flat surface on which to fabricate the electrodes. The electrodes were made by evaporating 0.5 μm of aluminum onto the smooth surface and then using standard photolithographic techniques to define the pattern. For

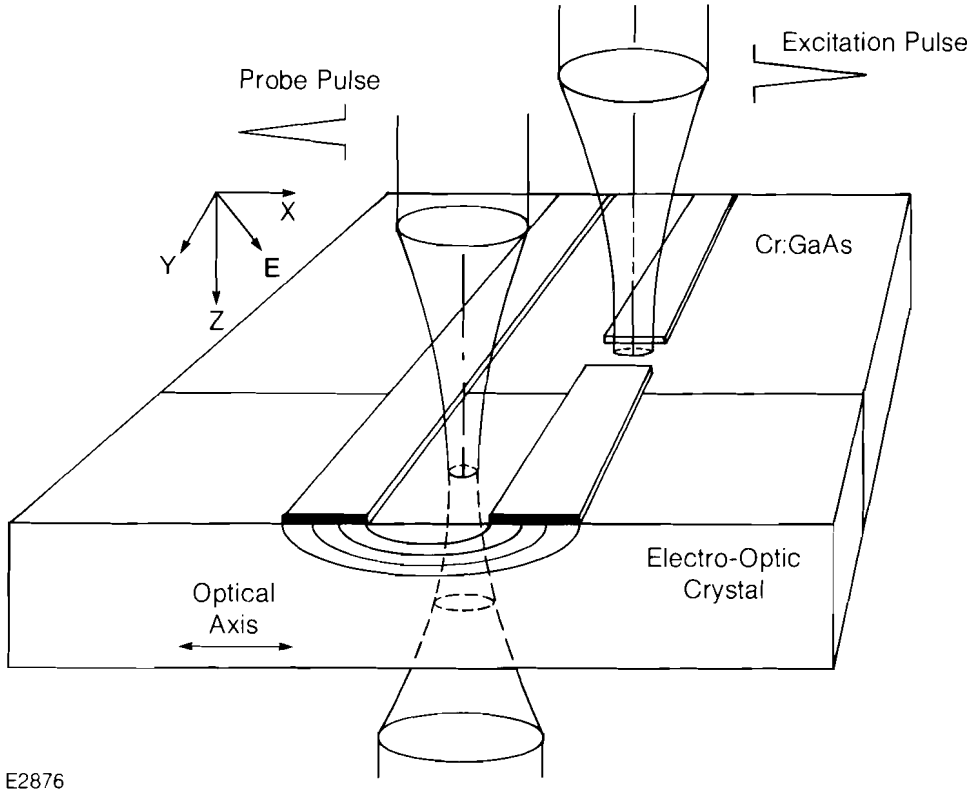

Fig. 19.20
Configuration of the coplanar strip electro-optic sampler. The signal is triggered photoconductively by the excitation pulse at the electrode gap on the Cr:GaAs substrate and probed by the perpendicular probe beam focused a short distance away in the $LiTaO_3$ crystal.

relative ease of fabrication we chose the electrode widths and separation to be 50 μm each. The calculated impedance for the line on the Cr:GaAs is 100 Ω and 56 Ω for the $LiTaO_3$.[4] The electrodes were made long enough (2 cm) to ensure that any reflection from the terminated end of the line arrived at the sampling point long after the initial rise of the electrical signal. The crystal optical axis of the lithium tantalate is parallel to the direction of the electric field between the electrodes, and, contrary to the standard configuration for integrated optical modulators, the probe beam is perpendicular to the electrode plane (see Fig. 19.20).

A typical result is shown in Fig. 19.21. In this case, the 50-μm gap was located 200 μm from the sampling point. The applied dc bias was +50 V. The probe beam was focused to a diameter of 11 μm between the two electrodes and was aligned perpendicular to the substrate. Temporal resolution did not appear to be significantly sensitive to the angle of incidence, which indicates that, as expected, the field depth in the substrate is very small and is of the order of the electrode separation. The resolved rise time (10%-90%), neglecting the foot on the leading edge due to dispersion, is 460 fs. The amplitude of the switched signal is 30 mV. The signal/noise ratio obtained indicates that the sensitivity of the coplanar strip geometry is comparable to that previously demonstrated with the balanced strip line.

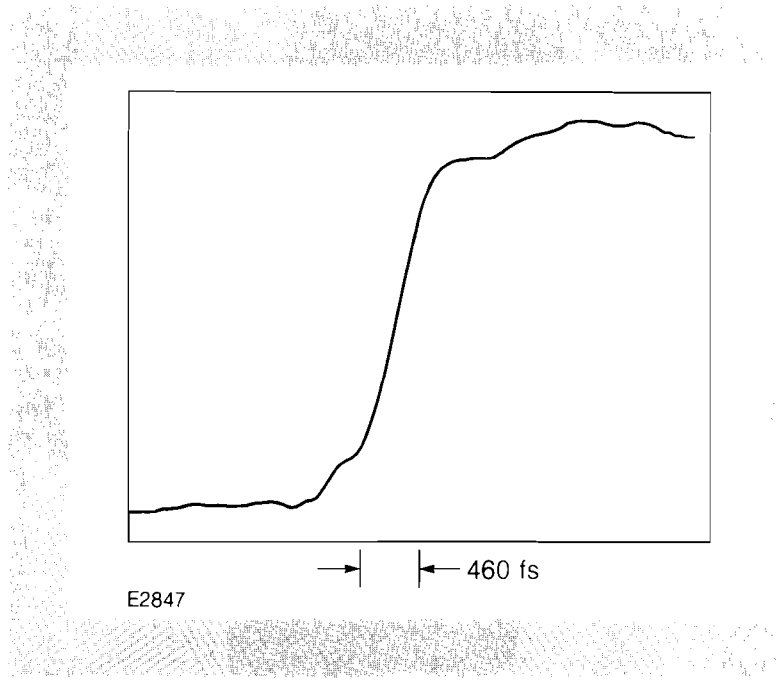

Fig. 19.21
Typical signal obtained with the electro-optic sampler, showing a rise time of 460 fs.

The observed rise time τ_S is the quadrature sum of the electrical pulse rise time τ_E, the transit time of the signal across the optical beam waist τ_W, the transit time τ_o of the optical pulse in the field region, and the laser pulsewidth τ_L:

$$\tau_S = \checkmark \tau_E^2 + \tau_W^2 + \tau_o^2 + \tau_L^2 .$$

The measured laser-beam waist is 11 μm, so $\tau_W \approx 230$ fs if we assume $\epsilon_{eff} \approx \epsilon_r = 40$ for very high frequencies and small geometries.[2] The laser pulse width $\tau_L = 120$ fs. If we equate τ_S with our experimental result of 460 fs, then we find $(\tau_E^2 + \tau_o^2)^{1/2} = 380$ fs which implies the limits $0 < \tau_E, \tau_o < 380$ fs. This allows us to place an upper limit of ~ 50 μm on the penetration depth of the electrical field into the substrate, which is in agreement with the strip-line geometrical parameters. The test-pulse rise time is ultimately limited, in the case of a uniformly irradiated gap, by the laser pulse width of 120 fs and by the dielectric relaxation time $\tau = \epsilon/\sigma$. The latter can only be estimated since we are in a regime of transient carrier velocities. In addition, due to the relatively high carrier concentration of 10^{17}-10^{18} cm^{-3}, band filling can occur resulting in an increase in optical penetration. If we assume a peak velocity of 5×10^7 cm/s,[9] an optical penetration depth of 1 μm, and 30 pJ/pulse, we calculate the dielectric time constant to be less than 50 fs.

The temporal resolution of the system may be further improved. The time τ_W may be reduced by reducing the focused diameter of the probe beam. The penetration of the electric field into the dielectric scales down with the separation of the electrodes, and to a lesser extent, with the electrode linewidths.[10] Reducing the dimensions of the strip line will increase the frequency response of the line and reduce the capacitance of the gap. These improvements are presently being incorporated into the experiment.

ACKNOWLEDGMENT

This work was supported by the following sponsors of the Laser Fusion Feasibility Project at the Laboratory for Laser Energetics—Empire State Electric Energy Research Corporation, General Electric Company, New York State Energy Research and Development Authority, Northeast Utilities Service Company, Southern California Edison Company, The Standard Oil Company, and University of Rochester. Such support does not imply endorsement of the content by any of the above parties.

REFERENCES

1. J. A. Valdmanis, G. A. Mourou, and C. W. Gabel, *IEEE J. Quantum Electron.* **QE-19**, 664 (1983).
2. J. A. Valdmanis, Ph.D. thesis, University of Rochester, 1983.
3. See, for example, K. C. Gupta, Ramesh Garg, and I. J. Bahl, *Microstrip Lines and Slot Lines* (Artech House, Inc., Dedham, MA, 1979), Chap. 7.
4. Cheng P. Wen, in *Parallel Coupled Lines and Direction Couplers*, edited by Leo Young, (Artech House, Inc., Dedham, MA, 1972), pp. 270-273.
5. Takeshi Hatsuda, *IEEE Trans. Microwave Theory Tech.*, **MTT-23**, 795 (1975).
6. D. Mirshekar-Syahkal and J. Brian Davies, *IEEE Trans. Microwave Theory Tech.*, **MTT-27**, 694 (1979).
7. Jeffrey B. Knorr and Klaus-Dieter Kuchler, *IEEE Trans. Microwave Theory Tech.*, **MTT-23**, 541 (1975).
8. Jayatna Venkataraman (private communication).
9. R. L. Fork *et al.*, *Picosecond Phenomena*, edited by C. V. Shank (Springer-Verlag, New York, 1980), Vol. II, p. 281.
10. Jeffrey B. Knorr (private communication).

3.B An Ultra-Stable Nd:YAG-Based Laser Source

A stable source is essential for the careful study of any nonlinear process. Current systems attain ± 5% energy stability from shot to shot.[1,2] A newly developed system operates much more consistently. Laser oscillator pulses from this system are stable to ± 0.8%, and amplified pulses (up to 100 mJ) are stable to ± 2%. The oscillator can operate at pulse rates up to 500 Hz and the amplifier up to 10 Hz.

Elements of the System

The system configuration is shown in Fig. 19.22. The oscillator is a continuously pumped Nd:YAG laser which is mode-locked and repetitively Q-switched at any rate between 0 and 500 Hz. The peak pulse in the 20- to 25-pulse FWHM output train has an energy of 120 μJ. A recently developed Pockels cell driver, capable of operating at repetition rates above 500 Hz, selects the peak pulse from

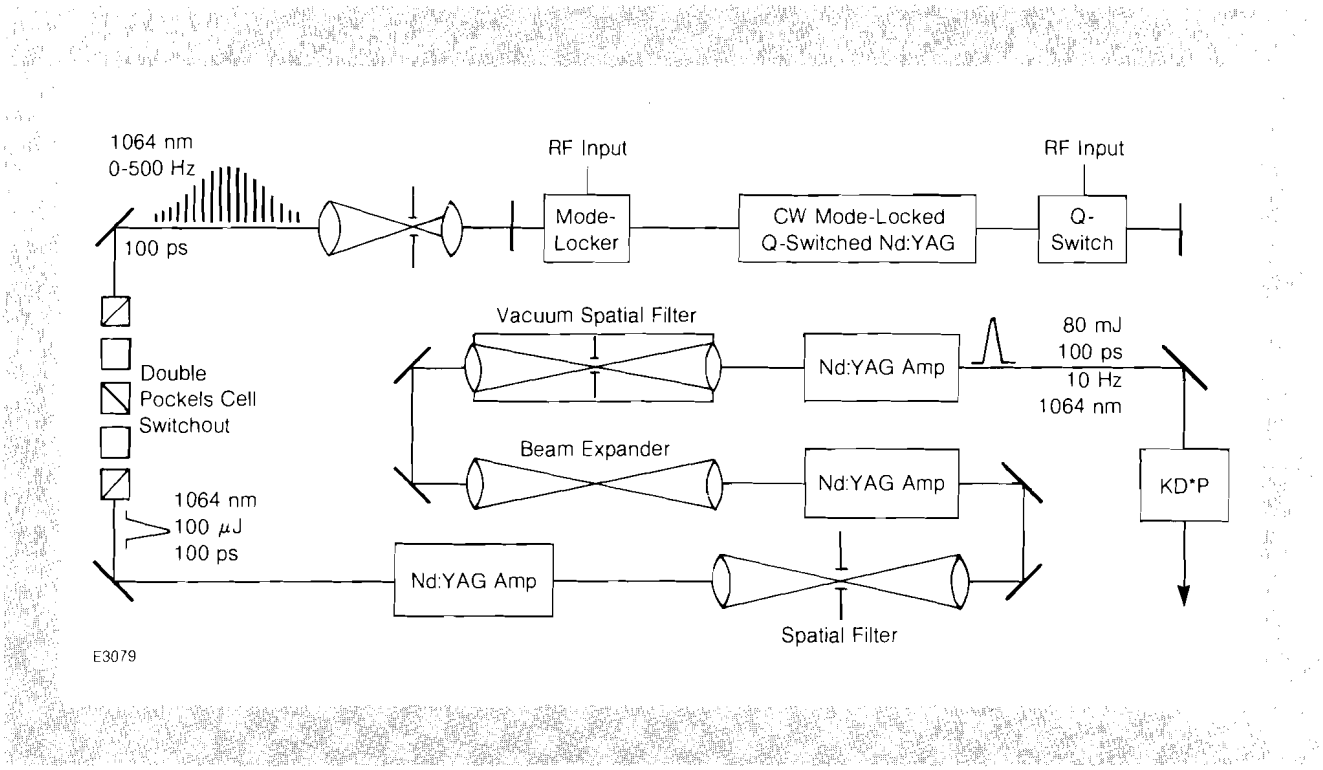

Fig. 19.22
System layout for the improved laser oscillator and amplifier.

the pulse train. This pulse propagates through three single-pass Nd:YAG amplifiers which are separated by spatial filters to maintain the beam quality. Output energies of as much as 100 mJ have been obtained at amplifier repetition rates up to 10 Hz. A doubling crystal may be inserted in the output beam as shown.

With continuous pumping, the oscillator operates at a low prelase level prior to the Q-switch. During the prelase period, transient relaxation oscillations decay (see Fig. 19.23), and the laser emission becomes fully mode-locked prior to Q-switching. This ensures that a consistent-amplitude, fully mode-locked pulse is present in the cavity when the laser is Q-switched. Thus, the prelase stabilizes the output pulse energy, duration, and build-up time. Output stability is further improved when the acousto-optic mode-locker and Q-switch are driven by the same rf source.

Resonant frequencies of the acousto-optic mode-locker vary significantly with temperature. We stabilize this device by regulating the input rf power and by cooling the acousto-optic crystals with a water bath regulated to 0.1°C.

Since the Q-switch is gated on a zero crossing of the RF, driving both the mode-locker and Q-switch from the same source defines the position of the pulse in the cavity when the Q-switch is triggered. In order to avoid undesirable interaction with the mode-locker, the Q-switch is placed in the optical center of the cavity.

The mode-locked laser is extremely sensitive to variations in the cavity length. To minimize thermally induced changes in the cavity

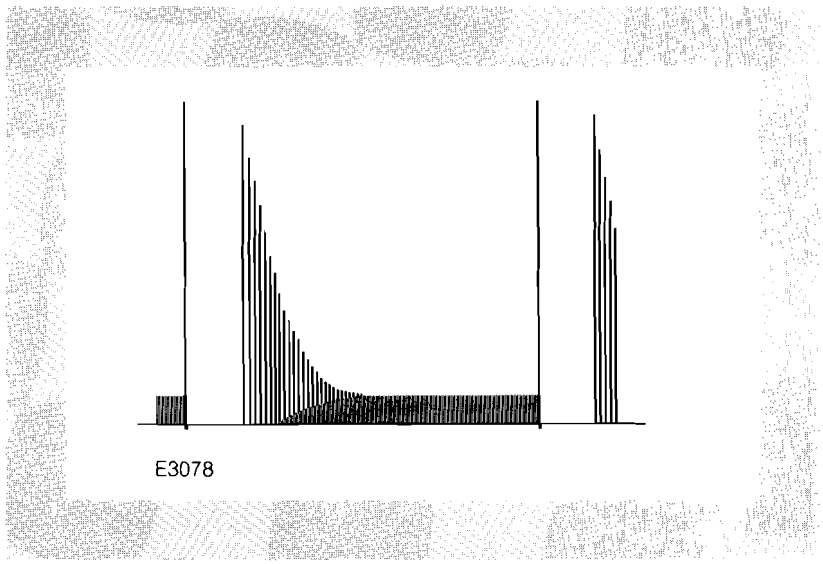

Fig. 19.23
Detail of the relaxation oscillation decay and prelase for the laser oscillator.

length, the end mirrors are mounted on a bar of Invar. The dc current to the arc lamp is also stabilized by an additional filtering capacitor and inductor to limit current fluctuations to less than 0.1%.

With these modifications this Nd:YAG oscillator produces a train of laser pulses, 25 pulses wide, with a peak pulse energy of 120 μJ at *any* repetition rate up to 500 Hz. The mode-locked pulse duration is measured at 100 ps.

The Pockels-cell switchout is driven by a new circuit developed to solve the short lifetime, limited repetition rate, and jitter problems of the krytron-driven switchout. The new design[3] incorporates a "hard" tube (microwave vacuum triode) whose grid is driven by a one- to two-transistor avalanche stack. The Pockels cell (PC) is built into the circuit package and is treated as a capacitor by the circuit. The circuit diagram is shown in Fig. 19.24.

The PC is charged to high voltage through a storage capacitor. The shunt resistance across the PC is adjusted to provide a 1- to 10-μs cell-discharge time constant. The PC capacitance is much less than the storage capacitance so the cell charges to full voltage when the tube conducts. Between firings, however, the PC potential returns to zero while the storage capacitor recharges.

Operation in this configuation produces a voltage function with a rise time of < 5 ns and a fall time of 1-10 μs. This function can be used either as a step-transmission function (if the final voltage is the half-wave voltage, $V_{\lambda/2}$) or as a switchout (if the final full-wave voltage is V_{λ} and the pulse is timed to correspond with the voltage passing through $V_{\lambda/2}$). When used as a switchout for a Q-switched laser, the second crossing of $V_{\lambda/2}$ (during the 1- to 10-μs decay) will occur after lasing has stopped.

In an alternate configuration, an avalanche transistor stack is connected across the PC (denoted by dashed lines in Fig. 19.24). The breakdown of this stack is adjusted so that it occurs when the

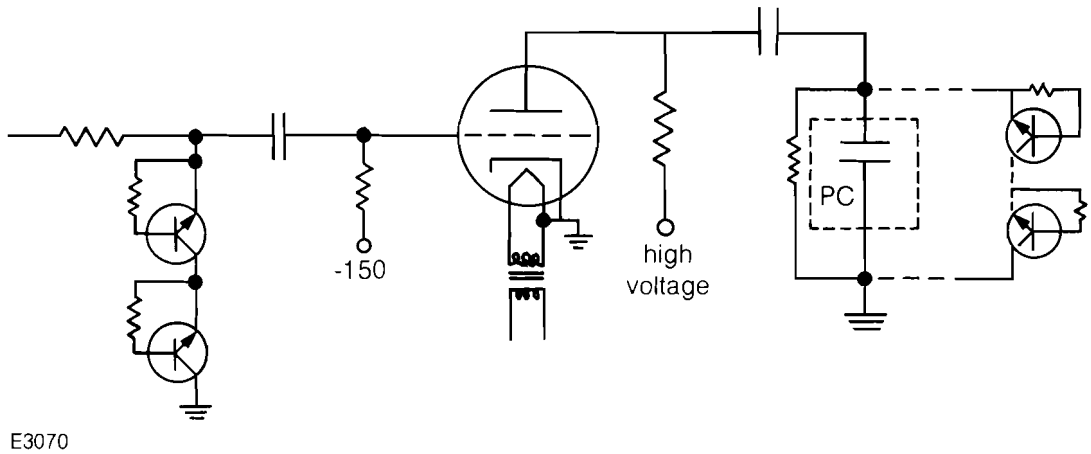

Fig. 19.24
Electrical schematic of the recently developed Pockels cell driver.

PC reaches $V_{\lambda/2}$. This option produces a PC voltage with a 5-ns rise, a ~ 5-ns fall, and a peak value of $V_{\lambda/2}$. This fast signal provides a 1- to 2-ns transmission window for pulse selection.

Timing for the PC trigger is accomplished by counting cycles of the mode-locker rf. Small adjustments are made by phase shifting the rf to the mode-locker. The total delay inserted is approximately 3 μs. The Q-switched buildup time is sufficiently stable to select the peak pulse consistently.

The shot-to-shot jitter is < 100 ps. There is also no apparent drift over weeks of operation. The tube is guaranteed to last for one year. At present over $2 \cdot 10^7$ shots have been accumulated with no apparent degradation. This performance is to be compared with that of a krytron switchout driver which has shot-to-shot jitter of > 1 ns, a lifetime drift of > 10 ns, and a tube lifetime of 10^7 shots. At a repetition rate of 500 Hz this allows approximately eight hours of operation. The new circuit design shows no change in performance as the repetition rate is increased. Rates as high as 1 kHz have been obtained, limited by only the power supplies and heat dissipation in the charging resistors.

The amplifier chain consists of three in-line amplifiers. The single pass gain of each can be as high as 30. Rod diameters in the first two heads are 7 mm. They are separated by an air spatial filter which maintains the beam quality and adjusts the beam size. Following the second amplifier is a focusing beam expander and a vacuum spatial filter. The output of the third (9-mm diam) amplifier is a 100-ps pulse of up to 100-mJ energy.

The IR pulse from the amplifier chain is frequency-doubled in an angle-tuned KD*P crystal. An overall energy conversion efficiency of 60% is routinely obtained. Both the green and the IR are used to drive experiments and detection equipment.

System-Operating Characteristics

The important characteristic of this system is the remarkable amplitude stability which results from combining the cw mode-locked, Q-switched Nd:YAG with the newly developed switchout. Figure 19.25 is a histogram of the normalized oscillator pulse energy for 1000 shots at 20 Hz. The average value is 100 with a full-width half-maximum of 1.6 which indicates a stability of ± 0.8%.

The process of amplification does add some fluctuation as illustrated in Fig. 19.26, a histogram of the amplified pulse energy. In the same manner the fluctuation is calculated as ± 2%.

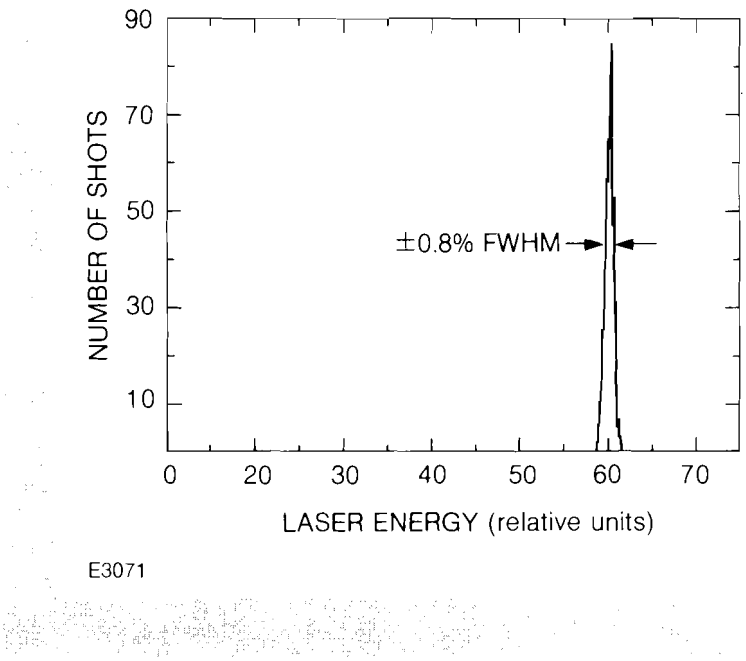

Fig. 19.25
Energy stability histogram for the laser oscillator and pulse selector.

Summary

The new laser source is exceptionally stable and operates at high repetition rates. Stability is attained because we have incorporated close control of the parameters that affect it into the design of the system. The new, hard-tube Pockels-cell driver enables high-repetition-rate operation.

This new source substantially increases our capability to measure rapid transient phenomena. The precision of statistical sampling techniques is improved by the stability of the source energy. Moreover, the high pulse energy extends the dynamic measurement range to lower levels.

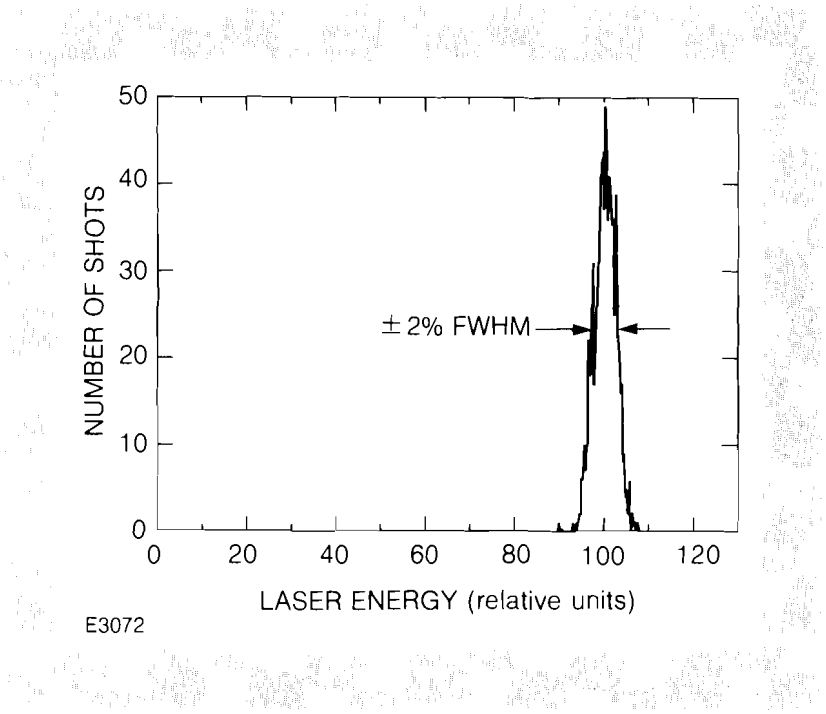

Fig. 19.26
Energy stability histogram for the amplified 1.06-μ laser pulse.

ACKNOWLEDGMENT

This work was supported by the following sponsors of the Laser Fusion Feasibility Project at the Laboratory for Laser Energetics—Empire State Electric Energy Research Corporation, General Electric Company, New York State Energy Research and Development Authority, Northeast Utilities Service Company, Southern California Edison Company, The Standard Oil Company, and University of Rochester. Such support does not imply endorsement of the content by any of the above parties.

REFERENCES

1. G. Albrecht and J. Bunkenburg, *Opt. Commun.* **38**, 377 (1981).
2. W. Seka and J. Bunkenburg, *J. Appl. Phys.* **49**, 2277 (1978).
3. T. Sizer, I. Duling, C. Petras, and S. Letzring, U.S. Patent Application No. 581144 (11 February 1984).

Section 4
NATIONAL LASER USERS FACILITY NEWS

This report covers the activities of the National Laser Users Facility (NLUF) during the quarter 1 April to 30 June 1984. During this period, four users conducted experiments on LLE facilities, and two users visited LLE to discuss their experiment. The visiting scientists who conducted experiments represented the Naval Research Laboratory and the University of Hawaii, and are listed below.

- R. Elton, T.N. Lee, and J. Ford
  (Naval Research Laboratory)
- P. Burkhalter, K. Hudson, W. Behring, and B. Dohne
  (Naval Research Laboratory)
- U. Feldman, J. Seely, and W. Behring
  (Naval Research Laboratory)
- B. Henke and P. Jaanimagi
  (University of Hawaii)

The two visiting users represented the Los Alamos National Laboratory and the University of California at Davis.

On April 20, 1984, the NLUF Steering Committee held its fifth meeting to review and approve proposals and to recommend funding of approved proposals in inertial fusion to the U.S. Department of Energy (DOE). This funding allocation is separate from LLE's operation contract and is designed to provide research funds to users in the inertial fusion field. Users in other fields may use the facility but must provide their own research funds.

Twenty-one proposals were submitted to the NLUF Steering Committee this year. The proposals were in a variety of areas including plasma physics, x-ray laser research, cryogenic targets, x-ray spectroscopy, instrumentation, nuclear fluorescence, and others. Ten of the twenty-one were approved. This year, three new user experiments were approved for facility time: **Carl Collins** (University of Texas at Dallas), **Dwight Duston** (Naval Research Laboratory), and **John DeGroot** (University of California at Davis). These new proposals represent 30% of the total approved number.

Ten of the proposals were approved for facility time. Individual funding levels for these experiments were recommended to DOE for their consideration. The committee noted the continued excellence of user experiments, that many of the proposals were from distinguished scientists, and that the top proposals were of high caliber.

The new approved proposals are listed below in alphabetical order.

1. **Philip G. Burkhalter** (Naval Research Laboratory)
   "X-Ray Spectroscopy to Determine Line Coincidences in High-Z Elements."
2. **Carl B. Collins** (University of Texas at Dallas)
   "Continuation of the Study of Nuclear Fluorescence Excited by Laser Plasma X-Rays."
3. **John S. DeGroot** (University of California at Davis)
   "Measurements of Parametric Instabilities Near the Critical Density and the Resultant Electron Heating."
4. **Dwight Duston** (Naval Research Laboratory)
   "Investigation of K-Shell Dielectronic Satellite Line Emission at Ultra-High Plasma Densities."
5. **Nizarali A. Ebrahim** (Yale University)
   "Studies of Parametric Instabilities in Hot Long Scale Length Plasmas."
6. **Uri Feldman** (Naval Research Laboratory)
   "A Proposal for Spectroscopic Studies Relevant to X-Ray Lasers Using the OMEGA Laser Facility."
7. **Hans R. Griem** (University of Maryland)
   "A Proposal for Thermal Transport Studies Using Extreme Ultraviolet Spectroscopy."
8. **Burton L. Henke** (University of Hawaii at Manoa)
   "Evaluation and Application of a Streak Camera and Photographic-Camera-Coupled Elliptical-Analyzer Spectrograph System for the Diagnostics of Laser-Produced X-Ray Sources (100–10,000-eV Region)."
9. **C.F. Hooper, Jr.** (University of Florida)
   "A Study of Plasma-Induced Continuum Lowering and Spectral Line Alterations: A Proposal to NLUF."
10. **Chan Joshi** (UCLA)
    "Studies of the Two-Plasmon Decay and Stimulated-Raman-Scattering Instabilities in 0.35-μm-Laser-Irradiated Plasmas."

ACKNOWLEDGMENT

This work was supported by the U.S. Department of Energy Office of Inertial Fusion under contract number DE-AC08-80DP40124.

PUBLICATIONS AND CONFERENCE PRESENTATIONS

Publications

H. Kim, T. F. Powers, and J. F. Mason, "Inertial Fusion Target Fabrication Using Polystyrene Mandrels," *J. Vac. Sci. Technol. A* **2**, 649-652 (1984).

M. C. Richardson, S. A. Letzring, W. Friedman, and G. Gregory, "Time-Resolved X-Ray Photography of Uniformly Irradiated Spherical Targets," *SPIE Proceedings, Vol. 427, High Speed Photography, Videography, and Phototonics*, 91-96 (1984).

M. C. Richardson, S. Skupsky, J. Kelly, L. Iwan, R. Hutchison, R. Peck, R. L. McCrory, and J. M. Soures, "Laser Fusion Target Irradiation Uniformity with the 24-Beam OMEGA Facility," *SPIE Vol. 380, Proceedings of the Los Alamos Conference on Optics '83*, 473-478 (1984).

R. W. Short, W. Seka, K. Tanaka, and E. A. Williams, "Two-Plasmon Decay and Three-Halves Harmonic Generation in Filaments in a Laser-Produced Plasma," *Phys. Rev. Lett.* **52**, 1496-1499 (1984).

B. Yaakobi, H. Kim, and J. M. Soures, "Summary Abstract: Submicron X-Ray Lithography Using Laser Produced Plasma as a Source," *J. Vac. Sci. Technol. A* **2**, 367-368 (1984).

S. Williamson, G. Mourou, and J. C. M. Li, "Time-Resolved Laser-Induced Phase Transformation in Aluminum," *Phys. Rev. Lett.* **52**, 2364-2367 (1984).

Forthcoming Publications

J. A. Abate, A. W. Schmid, M. J. Guardalben, D. J. Smith, and S. D. Jacobs, "Characterization of Micron-Sized, Optical Coating Defects by Photothermal Deflection Microscopy," to be published in *Proceedings of the 15th Annual Symposium on Optical Materials for High Power Lasers*.

W. E. Behring, J. F. Seely, S. Goldsmith, L. Cohen, M. C. Richardson, and V. Feldman, "Transitions of the Type 2s-2p in Highly Ionized Zn, Ga, and Ge," accepted for publication by *Journal of the Optical Society of America*.

R. S. Craxton and R. L. McCrory, "Hydrodynamics of Thermal Self-Focusing in Laser Plasmas," accepted for publication by *Journal of Applied Physics*.

J. M. Forsyth and R. D. Frankel, "An Experimental Facility for Nanosecond Time-Resolved, Low Angle X-Ray Diffraction Experiments Using a Laser-Produced Plasma Source," accepted for publication by *Review of Scientific Instruments*.

R. Keck, L. M. Goldman, M. Richardson, W. Seka, and K. Tanaka, "Observation of High Energy Electron Distributions in Laser Plasmas," accepted for publication by *Physical Review*.

S. Kacenjar, L. M. Goldman, A. Entenberg, and S. Skupsky, "$<\rho R>$ Measurements in Laser Produced Implosions Using Elastically Scattered Ions," accepted for publication by *Journal of Applied Physics*.

E. L. Lindman and K. Swartz, "Some Applications of the Hot Electron Transport Equation," to be published in the *1983 Proceedings for the CECAM Workshop on 'The Flux Limiter and Heat Flow Instabilities in Laser-Fusion Plasmas.'*

G. A. Mourou and K. E. Meyer, "Subpicosecond Electro-Optic Sampling Using Coplanar Strip Transmission Lines," accepted for publication by *Applied Physics Letters*.

N. S. Murthy and H. Kim, "Molecular Packing in Alkylated and Chlorinated Poly-p-Xylylenes," accepted for publication by *Polymer*.

A. Schmid, D. Smith, M. Guardalben, and J. Abate, "Photothermal-Deflection Analysis of UV Optical Thin Films," accepted for publication by *SPIE Volume 476, Technical Symposium East—Eximer Lasers, Their Applications and New Frontiers in Lasers*.

W. Seka, E. A. Williams, L. M. Goldman, R. W. Short, and K. Tanaka, "Convective Stimulated Raman Scattering Instability in UV Laser Plasmas," accepted for publication by *Physics of Fluids*.

J. M. Soures, review of *The High-Power Iodine Laser*, by G. Brederlow, E. Fill, and K. J. Witte, accepted for publication by *Journal of Quantum Electronics*.

K. Tanaka, W. Seka, L. M. Goldman, M. C. Richardson, R. W. Short, J. M. Soures, and E. A. Williams, "Evidence of Parametric Instabilities in Second Harmonic Spectra from 1054 nm Laser-Produced Plasmas," accepted for publication by *Physics of Fluids*.

Conference Presentations

R. L. Keck, "Short Wavelength Laser-Plasma Interaction Experiments in a Spherical Geometry," presented at the IEEE International Conference on Plasma Science, St. Louis, Missouri, May 1984 (invited talk).

A. Schmid, D. Smith, M. Guardalben, and J. Abate, "Photothermal-Deflection Analysis of UV Optical Thin Films," presented at the SPIE Technical Symposium East—Eximer Lasers, Their Applications and New Frontiers in Lasers, Alexandria, Virginia, May 1984.

S. D. Jacobs and A. W. Schmid, "Thin Film Defects and Laser Induced Damage," prsented at the DARPA/DEO Space Beam Control Technology Workshop, McLean, Virginia, May 1984.

W. Seka, "Laser-Plasma Interaction Experiments at 351 nm," presented at the Canadian Association of Physicists, Sherbrooke Conference, Quebec, Canada, June 1984.

A. Simon and R. Short, "A New Model of Raman Spectra in Laser Produced Plasma," presented at the International Conference on Plasma Physics, Lausanne, Switzerland, June 1984.

The following presentations were made at the Fourteenth Annual Anomalous Absorption Conference, Charlottesville, Virginia, May 1984:

O. Barnouin, J. Delettrez, L. M. Goldman, R. Marjoribanks, M. C. Richardson, J. M. Soures, and B. Yaakobi, "Thermal Transport Measurements in Six-Beam, UV Irradiation of Spherical Targets."

R. S. Craxton and R. L. McCrory, "Thermal Self-Focusing at Oblique Incidence."

J. Delettrez, R. Epstein, M. C. Richardson, and B. Yaakobi, "Limits on the Flux Limiter and Preheat from Simulations of Experiments on the OMEGA System at 1054 nm and 351 nm."

R. Epstein, S. Skupsky, J. Delettrez, and B. Yaakobi, "Non-LTE Considerations in Spectral Diagnostics of Thermal Transport and Implosion Experiments."

L. M. Goldman, W. Seka, K. Tanaka, A. Simon, and R. Short, "Observation of Scattered Light Between $\omega/2$ and $3\omega/2$ in Short Wavelength Laser Produced Plasmas."

R. S. Marjoribanks, M. C. Richardson, B. Yaakobi, O. Barnouin, J. Delettrez, R. Epstein, and W. Beich, "Time-Resolved Measurements of the Ionization Front in Transport Studies."

M. C. Richardson, R. Keck, B. Yaakobi, S. Letzring, J. Delettrez, C. Verdon, J. M. Soures, and G. Gregory, "Irradiation of Spherical Shell Targets with Six UV OMEGA Beams."

W. Seka, L. M. Goldman, K. Tanaka, B. Afeyan, A. Simon, and R. Short, "How Useful are Odd-Integer Half-Harmonics?"

R. W. Short and K. Swartz, "Localized Heat Flow Instabilities in Laser Plasmas."

A. Simon, C. J. McKinstrie, and E. A. Williams, "Nonlinear Saturation of the Parametric Instability for Three Coupled Oscillators."

A. Simon and R. W. Short, "A New Model of Raman Spectra in Laser Produced Plasma."

S. Skupsky and J. Delettrez, "The Effect of Thermal Flux Saturation on Lateral Heat Transport — a Multi-Group Analysis."

K. Swartz and R. W. Short, "Nonlocal Heat Transport by Non-Maxwellian Electrons."

K. Tanaka, B. Boswell, R. S. Craxton, L. M. Goldman, M. C. Richardson, W. Seka, R. W. Short, and J. M. Soures, "Brillouin Scattering in Underdense UV Laser-Produced Plasmas."

The following presentations were made at the Topical Meeting on Ultrafast Phenomena, Monterey, California, June 1984:

K. E. Meyer and G. A. Mourou, "Subpicosecond Electro-Optic Sampling Using Coplanar Strip Transmission Lines" (invited talk).

T. Norris, T. Sizer, and G. Mourou, "Generation of 90 fs Pulses with a CPM Laser Pumped by a Frequency-Doubled CW Mode-Locked Nd:YAG."

S. Williamson, G. Mourou, and J. C. M. Li, "Time-Resolved Laser-Induced Phase Transformation in Aluminum."

The following presentations were made at the Conference on Lasers and Electro-Optics, Anaheim, California, June 1984:

W. Beich, M. Dunn, R. Hutchison, L. Iwan, S. Jacobs, L. Lund, R. Peck, D. Quick, M. C. Richardson, F. Rister, and J. M. Soures, "Performance Characterization of the OMEGA Short-Wavelength Laser Facility."

L. Iwan, D. Quick, W. Seka, and K. Walsh, "A System to Measure the Output Energy of a Frequency-Tripled Neodymium Glass Laser."

J. Kelly and D. Smith, "Beam Profile Control on the OMEGA Laser System."

T. J. Kessler and J. M. Forsyth, "Holographic Recording of a Pulsed High Power Laser."

K. E. Meyer and G. A. Mourou, "Subpicosecond Electro-Optic Sampling Using Coplanar Strip Transmission Lines."

M. C. Richardson, S. Skupsky, J. M. Soures, W. Lampeter, S. Tomer, R. Hutchison, M. Dunn, and W. Beich, "Irradiation Uniformity with Multiple Beam UV Irradiation Facility."

J. F. Whitaker, T. Norris, and G. Mourou, "Pulse Shaping in Dispersive Transmission Lines."

I. N. Duling, P. Bado, S. Williamson, G. Mourou, and T. Baer, "A Stable Kilohertz Nd:YAG Regenerative Amplifier."

The following presentations were made at the Thirteenth International Conference on Quantum Electronics, Anaheim, California, June 1984:

M. C. Richardson, O. Barnouin, R. S. Craxton, J. Delettrez, R. L. Keck, R. S. Marjoribanks, W. Seka, J. M. Soures, and B. Yaakobi, "Absorption Physics at 351 nm in Spherical Geometry."

W. Seka, R. W. Short, L. M. Goldman, S. Letzring, M. C. Richardson, J. M. Soures, K. Tanaka, R. S. Craxton, J. Delettrez, R. Boni, and D. Quick, "Half-Integer Harmonic Emission from Laser Plasmas as Coronal Temperature Diagnostic."

T. Sizer II and M. G. Raymer, "Picosecond Optical Collisions."

K. Tanaka, B. Boswell, R. S. Craxton, L. M. Goldman, M. C. Richardson, W. Seka, R. W. Short, and J. M. Soures, "Self-Focusing in Underdense UV Laser-Produced Plasmas."

S. Williamson, G. Mourou, and J. C. M. Li, "Time-Resolved Laser-Induced Phase Transformation in Aluminum."

T. Norris, T. Sizer, and G. Mourou, "Generation of 90 fs Pulses with a CPM Laser Pumped by a Frequency-Doubled CW Mode-Locked Nd:YAG."

The work described in this volume includes current research at the Laboratory for Laser Energetics which is supported by Empire State Electric Energy Research Corporation, General Electric Company, New York State Energy Research and Development Authority, Northeast Utilities Service Company, Southern California Edison Company, The Standard Oil Company, University of Rochester, and the U.S. Department of Energy Office of Inertial Fusion under contract DE-AC08-80DP40124.